SECTION A

CHAPTER 1

INTRODUCTION

1.1. General Overview of Thesis: Problem Statement

1.1.1. Self-assembly in electrode fabrication

Self-assembly is simply the term used to describe a spontaneous organization process of molecular units into ordered structures on metallic surfaces. The interaction responsible for the formation of the self-assembled system acts directly on the nanostructure architecture. Self-assembly can be classified as either static or dynamic. However, there are three distinctive features that make self-assembly a distinct concept, namely order, interactions and building blocks. Self-assembled monolayer (SAM) modified electrodes represent a modern approach to electrode systems. Presently, self-assembly technique is used to modify electrodes by anchoring inorganic or organic entities onto the electrode surface.

These electrodes rely on the placement of a molecular reagent onto the surface, to impart the behavior of that reagent to the modified surface. Such deliberate alteration of electrode surface can thus meet the needs of many electroanalytical problems and may form the basis for new analytical applications and different sensing devices. SAM technique has a number of advantages over other monolayer formation techniques which include simplicity, reproducibility and formation of highly ordered and stable monolayer which are chemically

bound onto solid surface. The use of SAM for the fabrication of electrodes with redox-active materials such as SWCNT and phthalocyanine is hugely unexplored.

1.1.2. Carbon nanotubes as electron-conducting nanowires

Since the re-discovery of carbon nanotubes in 1991 by Iijima [1], following the original discovery by Wiles and Abrahamson in 1978 [2], carbon nanotubes (CNT) have become an increasingly important group of nanomaterials with unique properties such as geometry, electronic, mechanical and chemical properties. Over the years, new discoveries have led to new applications, often taking advantage of these unique properties in different fields such as nanotechnology, electronics, optics and material science.

CNTs were first applied in electrochemical sensing in 1996 by Britto and co-workers [3], and since then research on their potential applications in electrochemistry has continued to grow in leaps and bounds. These potential applications in electrochemistry are made possible by the high electrochemically accessible surface area of porous nanotube arrays, combined with their high electronic conductivity and useful mechanical properties. Carbon nanotubes display metallic, semiconductive and superconducting electron transport, thus provide direct electrical communication between the

underlying electrode and the redox active species with no need for redox mediators [4,5]. Despite the excellent physico-chemical properties of CNTs, their immobilization onto electrode surfaces via SAM is hugely unexplored. Carbon nanotubes were used in this project as electron-conducting nanowires to enhance the electrochemical performance of organo-iron electrocatalyst (iron containing complexes).

1.1.3. Metallophthalocyanines as electrocatalysts

Metallophthalocyanines (MPcs) are metal N4-macrocyclic organometallic complexes that have found applications in a plethora of area. Most of the applications of MPc complexes arise from their diverse chemical, structural, electronic and optical properties. This is mainly because of their chemical stability [6].

Electroanalytical characterization of MPc and transition metal phthalocyanine (MPc) complexes has been an area of intense research. These complexes are well known robust and versatile electrocatalysts for the reduction and oxidation of a number of molecules of biological, biomedical clinical, pharmaceutical, industrial and environmental importance [6]. Their electrocatalytic activity lies in their ability to easily bind one or two axial ligands, especially analytes and undergo either metal-centered, ring-centered or axial ligand-centered redox

reactions [6-11]. Research has revealed that chemically modified electrode improves catalytic current necessary for sensitive detection of target analytes. As a result, the MPc based modified electrodes have exhibited enhanced sensitivity and selectivity of analytes [12]. Thus, this thesis focuses on the applications of modified electrodes fabricated with MPc, notably iron(II)Pc (FePc) complexes as well as ferrocenes. The co-intergration of MPc and CNTs as electrode modifiers is rarely reported and the electron transport is almost unknown.

1.1.4. Carboxylated ferrocenes as electrocatalysts

Ferrocene (Fc) is a coordination compound which falls under the supramolecular chemistry and its applications permitted their fast and spontaneous incorporation to nanosystems [13]. Building coordination compound on solid surfaces has made the preparation of nanoscaled devices with new properties possible. Ferrocene-terminated self-assembled monolayers are redox-active two dimensional aggregates on metal surfaces. These SAMs have been used as convenient, robust and well-reproducible surface self-assemblies for the kinetic and thermodynamic studies of electron transfer [14,15] and the influence of the redox environment on electron transfer kinetics [16,17]. Gooding *et al*. [18] have measured the electrochemical characteristics of ferrocenemethylamine modified single-walled carbon nanotubes

immobilized to a self-assembled monolayer of mercaptoethylamine on gold electrode. However, the co-assembling of SWCNTs and ferrocenes are not known. This work also examines for the first time the electrochemical and electrocatalytic properties of mixed SAMs of SWCNTs and Fcs.

1.1.5. Aim of thesis

Self-assembled monolayer (SAM) technique is well recognized as an efficient electrode fabrication strategy for forming stable, well-organised, ultrathin films of thiol-derived molecular species. Stable immobilization of redox-active materials, such as carbon nanotubes, transition metallophthalocyanines and ferrocenes, as ultrathin films on solid substrate is important for the development of several technological devices such as sensors, electronic device, catalyst, etc.

The development of chemical sensors is currently one of the most active areas of analytical research. Electrochemical sensors represent an important subclass of chemical sensors in which an electrode is used as the transduction element. Such device hold a leading position among sensors presently available, have reached a commercial stage (i.e screen printed electrodes) Despite the excellent physico-electrochemical properties of carbon nanotubes,

metallophthalocyanines and ferrocenes in the literature, their immobilization onto electrodes via SAM process is virtually unknown. The main objectives of this project therefore are:

(a) To integrate the redox-active species (i.e., carbon nanotubes, iron-phthalocyanines and ferrocenes) as ultrathin films on electrodes using SAM technique.

(b) Interrogate the integrity of such CNT-FePc or CNT/Fc hybrid in terms of:

(i) Heterogeneous electron transfer dynamics, and

(ii) Electrocatalysis of biologically and environmentally important analytes (thiocyanate).

In this introductory chapter, I will give a general overview of electrochemistry, electrochemical techniques, electrode modification processes, carbon nanotubes, phthalocyanine complexes, ferrocene complexes, analytes (thiocyanate and epinephrine) used in this work as analytical probes. Chapter two provides the procedures adopted for the experiments. Finally, chapters three to six will discuss the results obtained.

1.2. Overview *of Electrochemistry*

1.2.1. Basic concepts

Electrochemistry is the branch of chemistry that studies the interplay between chemical reactions and electricity. The fundamental process in electrochemical reactions is the transfer of electrons between the electrode surface and molecules in the interfacial region, either in solution or immobilized at the electrode surface. Therefore, electrochemistry is one effective technique to study electron transfer properties. When electron transfer is between a solid substrate and a solution species, it is termed heterogeneous process. Inversely, if electron transfer reaction occurs between two species, both of which are in solution, the reaction is homogeneous.

Electrochemistry involves the measurement of potential (potentiometry) or current response (voltammetry) [19]. The work described in this thesis involves current measurement, voltammetry and a number of voltammetric techniques, namely, cyclic voltammetry (CV), square wave voltammetry (SWV), chronoamperometry (CA) and linear sweep voltammetry (LSV).

1.2.2. The electrode-solution interface

Charged particles exist at every material interface called the *electrical double layer*. In electrochemistry, this layer reflects the ionic zones formed in the solution to compensate for the excess of charge on the electrode. The model produced by stern [20] which describes double layer is made up of several layers, when the electrode is immersed in solution as illustrated in figure1.1. Whether the charge on the metal is negative or positive with respect to the solution depends on the potential across the interface and the composition of the solution. A positively charged electrode thus attracts a layer of negative ions and vice versa. The inner layer closest to the electrode contains solvent molecules that are specifically adsorbed on the electrode. This layer is called the *Inner Helmholtz Plane* (IHP) or *compact layer* [21]. The outer layer called the *Outer Helmholtz Plane* (OHP) is the imaginary plane passing through the solvated cations. These planes cannot be measured nor do they exist so it can be assumed that the distance from the electrode to the IHP indicated as x_1 will be the radius of the ion and the solvated ions can approach the metal only at a distance x_2. The layer which extends from the OHP into the bulk solution is a three dimensional region of scattered ions called the diffuse or Gouy layer.

The IHP and OHP represent the layer of charges which is strongly held by the electrode and can survive even when the electrode is pulled out of the solution [21,22].

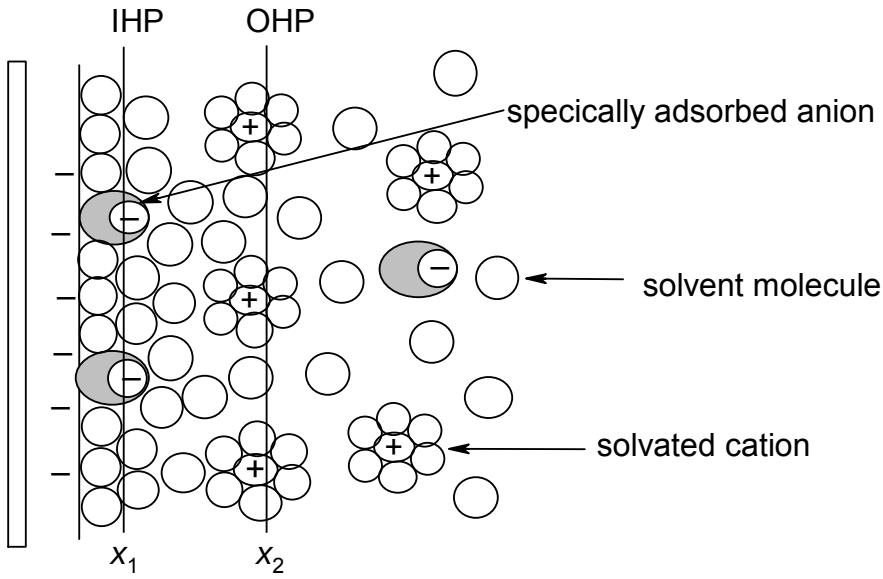

Figure 1.1: Model of the electrode-solution double layer regions in a case of a negatively charged electrode.

1.2.3. Faradaic and Non-Faradaic process

Oxidation and reduction processes are governed by Faraday's law which states that the amount of chemical reaction caused by the flow of current is proportional to the amount of electricity passed.

These reactions are called Faradaic processes as electrons are transferred across the metal-solution interface. Non-Faradaic process arise when an electrode-solution interface shows a range of potentials

where no charge-transfer reactions occur. However, processes such as adsorption and desorption can occur, and the structure of the electrode-solution interface can change with changing potential or solution composition. Although charge does not cross the interface, external currents can flow (at least transiently) when the potential, electrode area, or solution composition changes.

1.2.4. Mass transport processes

Mass transport is a process which governs the movement of charged or neutral species and contributes to the flow of electricity through an electrolyte solution in an electrochemical cell. This movement is considered as mass transfer of an electroactive species near the electrode by using a supporting electrolyte and operating in a quiescent solution. **Migration**, **diffusion** and **convection** are the three possible mass transport processes accompanying an electrode reaction.

(a) Migration

Migration is the type of charge transport that is related to the movement of ions and the existence of potential gradient between two electrodes in solution [23]. Controlled-potential experiments require a

supporting electrolyte to decrease the resistance of a solution and eliminate electromigration effects to maintain a constant ionic strength. To eliminate or suppress electromigration, addition of excess or large concentration of inert salt such as KCl is used in this work. In analytical applications, the presence of a high concentration of supporting electrolyte which is hundred times higher than the concentration of electroactive ions means that the contribution of examined ions to the migrational transport is less than one percent. Then it can be assumed that the transport of the examined species towards the working electrode is by diffusion only. Migration of electroactive species can either enhance or diminish the current flowing at the electrode during reduction or oxidation of cations. It helps reduce the electrical field by increasing the solution conductivity, and serves to decrease or eliminate sample matrix effects. The supporting electrolyte ensures that the double layer remains thin with respect to the diffusion layer, and it establishes a uniform ionic strength throughout the solution. However, measuring the current under mixed migration-diffusion conditions may be an advantage in particular electrochemical and electroanalytical situations [24].

(b) Diffusion

Diffusion is the transport of particles as a result of local difference in the chemical potential [25]. Diffusion is simply the movement of material from a high concentration region of the solution to a low concentration region. If the potential at an electrode oxidizes or reduces the analyte, its concentration at the electrode surface will be lowered, and therefore, more analyte moves to the electrode from the bulk of the solution, which makes it the main current-limiting factor in voltammetric process.

Although migration carries the current in the bulk solution during electrolysis, diffusion should also be considered because, as the reagent is consumed or the product is formed at the electrode, concentration gradient between the vicinity of the electrodes and the electroactive species arise. Indeed, under some circumstances, the flux of electroactive species to the electrode is due almost completely to diffusion.

(c) Convection

Convection is one of the modes of mass transport which involves the movement of the whole solution carrying the charged particles. Forced convection, which can also occur, may be unintentional and occurs as a result of vibrating building but usually, stirring is applied to

enhance the rate of mass transport process [26]. Stirring can be achieved by stirring the solution with the help of a separate stirrer or most conveniently, the use of rotating disk electrode is used for the purpose of convection. In voltammetry, convection is eliminated by maintaining the cell under quiet and stable condition.

1.3. Voltammetric techniques

As already stated, voltammetry alone was employed in this project, namely, Cyclic voltammetry (CV), Square wave voltammetry (SWV), Chronoamperometry (CA) and linear sweep voltammetry (LSV). This section gives the basic theoretical background underlying these techniques.

1.3.1. Cyclic voltammetry

Cyclic voltammetry (CV) is often the first experiment performed in an electroanalytical study, particularly due to its ability to rapidly provide considerable information on the thermodynamics of redox processes and the kinetics of heterogeneous electron transfer reactions. It offers a rapid location of redox potentials of the electroactive species and convenient evaluation of the effect of electrolyte on the redox process. There are three cyclic voltammetric processes that could take place, namely, reversible, irreversible and quasi-reversible.

1.3.1.1 Reversible process

The amount of the oxidized species at the electrode surface become reduced by the reduction process and replaced by the reduced

species, which diffuses away into the solution. If we reverse the potential sweep process from the positive side, the reverse effect is observed. As the potential sweeps reverses back towards the redox potential, then the reduced species will start to be re-oxidized. The current will then increase in the negative direction until an oxidation peak is reach. Figure 1.2 indicates the resulting scan of potential against time, scanning linearly the potential of a stationary working electrode in an unstirred solution, using a triangular potential waveform. The potentiostat measures current resulting from the applied potential.

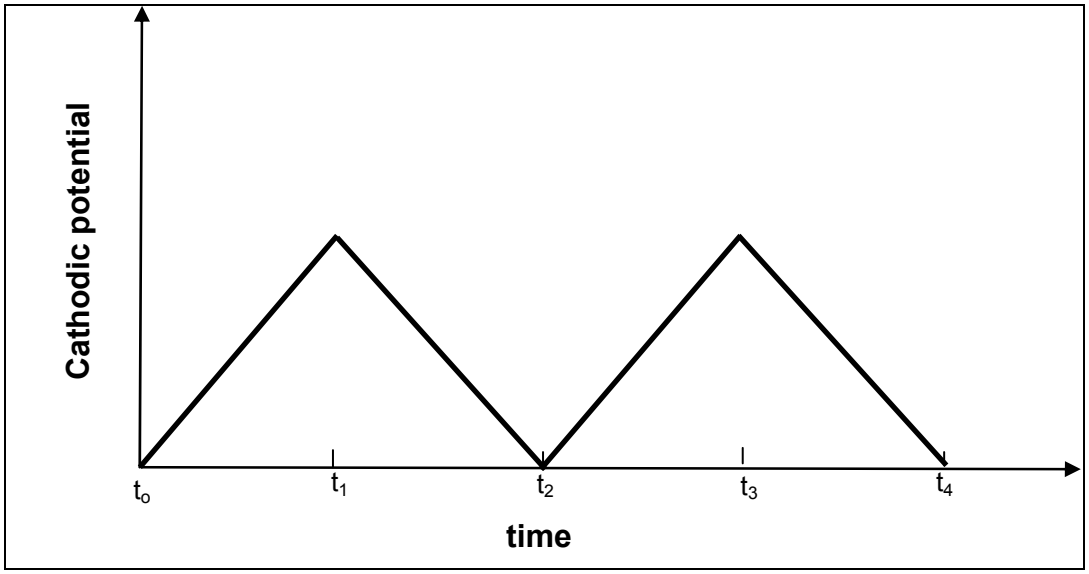

Figure 1.2: The potential waveform applied to W.E in the cyclic voltammetry experiment.

The potentiostat is controlled by a computer which enables one to analyze the current-potential plot called cyclic voltammogram. The expected cyclic voltammogram of a reversible redox couple for a single potential cycle is illustrated in Figure 1.3.

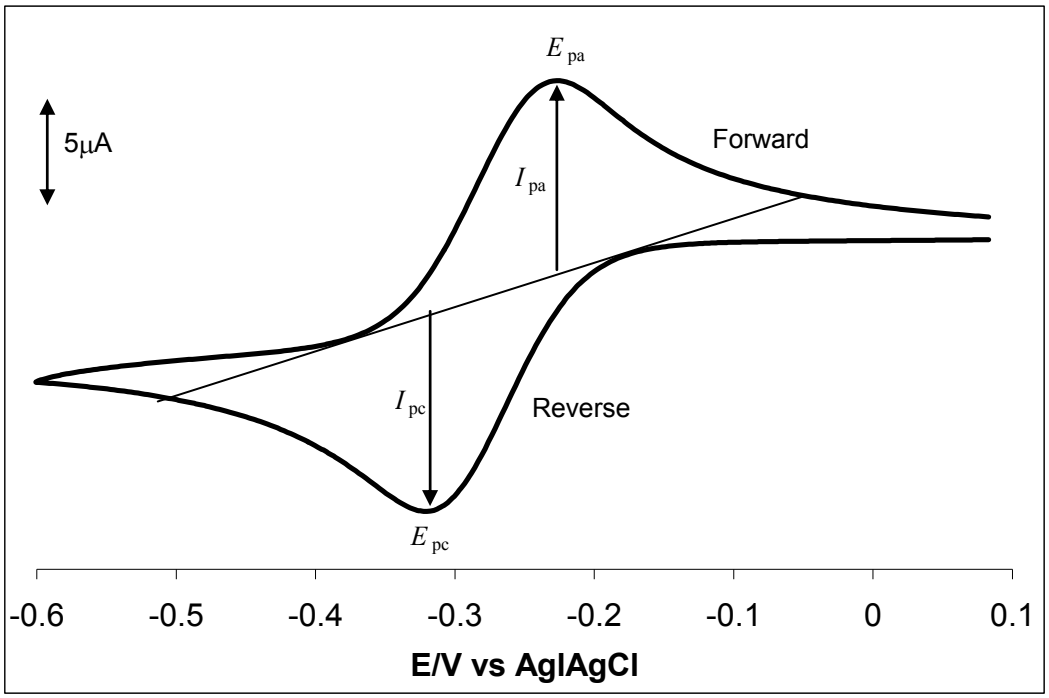

Figure 1.3: Typical cyclic voltammogram for a reversible redox process.

Closer look at figure 1.3, it is assumed that only the oxidized form (analyte or electrolyte) is initially present, therefore a potential scan in the negative direction is chosen for the first half-cycle, starting from a point where no reduction occurs. As the applied potential approaches E^o, the standard potential, for a redox process, a cathodic current begins to increase until a peak reaches maximum. The

potential at which the peak current occurs is known as the peak potential, E_p. At this potential, the redox species has been depleted at the electrode surface and the current is diffusion limited. After potential region in which the reduction process takes place, the direction of the potential scan is reversed. During this scan, the R molecules generated in the forward half-cycle and accumulated near the surface, are reoxidized back to O, resulting in the anodic peak. The magnitude of the Faradaic current, called the anodic peak current, I_{pa}, or cathodic peak current, I_{pc}, is indicative of rate of electron transfer between the electrode and the redox species. The electrical signal is related to the recognition process and is proportional to the concentration of the analyte. To clearly simplify the direction undertaken by the electron, Bard and Faulkner [24] explained that by driving the electrode to negative potentials, the energy of the electrons is raised high enough to transfer into the vacant electronic state on species in the electrolyte i.e the reduction current, thus a flow of electrons from electrode to solution occurs. Similarly, by imposing a more positive potential, the energy of the electrons is lowered and electrons in the electrolyte will transfer to the electrode i.e oxidation current. The flow of the electrons to and from the electrode surface is governed by mass transport.

For a reversible process, the Nernst equation is obeyed in which the electron transfer is fast, allowing the assumption that the concentration of both the oxidized, O and reduced, R species are in a state of equilibrium, equation 1.1.

$$O + ne^- \leftrightarrows R \qquad (1.1)$$

The electroactive species are stable thus the magnitude of the reverse-to-forward peak current ratio is unity for a simple reversible couple. The peak-to-peak separation (ΔE_p) should be independent of the scan rate, *v*, but in practice it slightly increase with *v*, this is due to the solution resistance, R_s, between the reference and working electrode [27]. The peak current, I_p of a reversible process is given by the Randles-Sevčik equation 1.2 [24]:

$$I_p = (2.69 \times 10^5)\, n^{3/2} A D^{1/2} C v^{1/2} \qquad (1.2)$$

where n is the number of electrons, A the area of the electrode in cm^2, C the concentration in $mol.cm^{-3}$, D the diffusion coefficient in cm^2s^{-1} and *v* the potential scan rate in Vs^{-1}. The current I_p, is directly proportional to concentration of the analyte [5] and increases with the square root of the scan rate. The dependence of current on the scan rate is indicative of electrode reaction controlled by diffusion [28-30],

using equation 1.2 a linear plot of I_p vs. $\nu^{1/2}$ is obtained. Deviation from linearity indicates the presence of chemical reaction involving either the oxidized, reduced or both species.

For a reversible process, the half-wave potential, $E_{1/2}$, equals the formal potential $E^{o'}$ and are related to the standard potential (E^o) as in equation 1.3:

$$E_{1/2} = E^{o'} = E^o + \frac{RT}{2nF}\ln\frac{[O]}{[R]} \qquad (1.3)$$

where R is the gas constant, T the temperature in Kelvin, F the Faraday's constant and [**O**] is the concentration of oxidised species, [**R**] is the concentration of reduced species in mol l^{-1}, respectively. The formal redox potential, $E^{o'}$ can be calculated from equation 1.4:

$$E_{1/2} \text{ or } E^{o'} = \frac{E_{pa} + E_{pc}}{2} \qquad (1.4)$$

where E_{pa} is the anodic peak potential and E_{pc} is the cathodic peak potential. The number of electrons transferred in a reversible process can be calculated from equation 1.5:

$$\Delta E = E_{pc} - E_{pa} = \frac{RT}{nF} \text{ , at } 25^0\text{C}$$

$$\Delta E = \frac{0.059\ V}{n} \qquad (1.5)$$

where n is the number of electrons transferred, other symbols have their usual meaning. The peak-to-peak separation is approximately 59 mV at 298 K and is independent of scan rate.

1.3.1.2 Irreversible process

Totally irreversible processes usually are due to slow electron exchange or slow chemical reaction at the electrode surface [31]. These processes are characterized by a shift of the peak potential with the scan rate and Δ*E* can be calculated from equation 1.6:

$$\Delta E = E^o - \frac{RT}{\alpha n_a F}\left[0.78 - \ln\frac{k^o}{D^{1/2}} + \ln\left(\frac{\alpha n_a F \nu}{RT}\right)^{1/2}\right] \qquad (1.6)$$

where α is the rate of electron transfer and n_a is the number of electrons involved in the charge transfer step and k^o is the heterogeneous electron transfer coefficient in cms^{-1}. The other symbols are listed in the list of symbols. At 25°C, the peak potential and the half-peak potential differ by 0.048 V/α*n*. Hence, the voltammogram becomes more drawn-out as α*n* decreases. In an irreversible process, only forward for oxidation or reverse reduction peak is observed, see Figure 1.4. It is common to observe a weak reverse peak at increased scan rates during forward oxidation at times, because of sluggish electron exchange as mentioned above. The

Nernst equation is not applicable in the case of irreversible process. This is due to the rate of electron transfer insufficient to maintain surface equilibrium and thus the oxidized and reduced species are not at equilibrium.

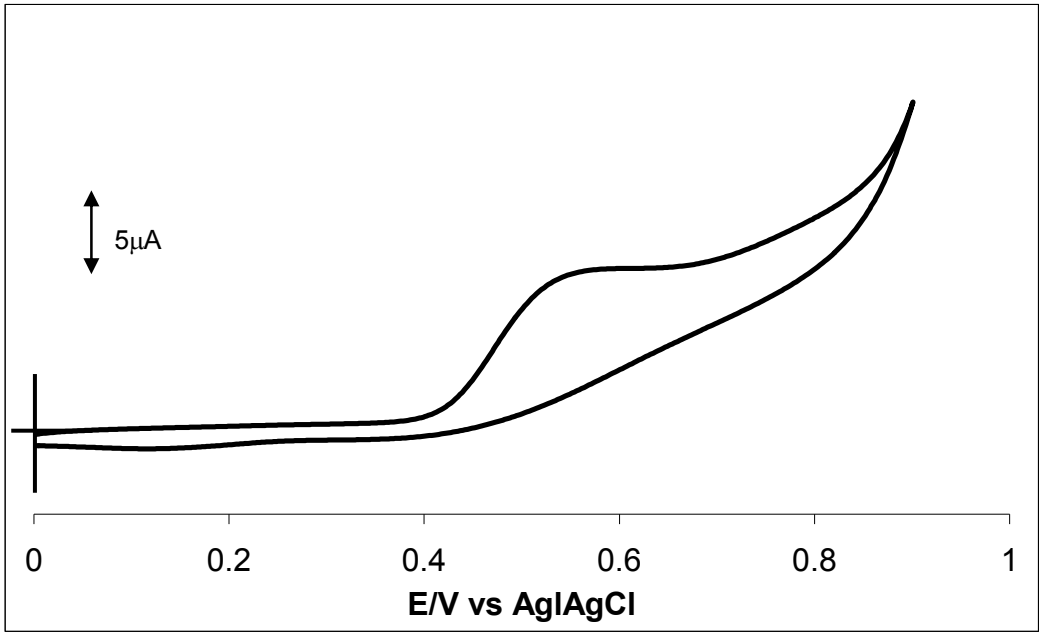

Figure 1.4: Typical cyclic voltammogram for an irreversible process.

The peak current, I_p for an irreversible process can be calculated from equation 1.7:

$$I_p = \left(2.99x10^5\right)n\left[(1-\alpha)n\right]^{1/2} ACD^{1/2}\nu^{1/2} \qquad (1.7)$$

The peak current is proportional to the bulk concentration but is lowered in height by the value of α, which is assumed to be 0.5.

Overall the cyclic voltammetric set up consist of the working electrode (W.E.), a counter electrode (C.E.) and a reference electrode (R.E.) immersed in a quiescent solution. The solution is kept stationary to avoid movement of ions to the electrode by mechanical means.

1.3.1.3 Quasi-reversible process

Mass transport plays a major role in controlling the concentration of the redox couple and the expressions for reversible processes also apply for quasi-reversible processes. The voltammograms of a quasi-reversible process exhibit a large peak-to-peak separation compared to reversible processes. The peak current increase with $v^{1/2}$ but is not linear and ΔE is greater than 0.0059/n V. In reversible process, current is controlled purely by mass transport but in quasi-reversible process, current is controlled by both the mass transport and charge transfer kinetics [31,32]. Table 1.1 summarizes the slight differences in cyclic voltammetric processes.

Table 1.1: The diagnostic criteria for reversible, irreversible and quasi-reversible cyclic voltammetric processes [24,28,33].

Parameters	Cyclic Voltammetry Process		
	Reversible	Irreversible	Quasi-reversible
E_p	Independent of v	Shift cathodically by $30/\alpha n$ mV for 10-fold increase in V	shift with v
E_{pc} - E_{pa}	$\approx 59/n$ mV at 25^0C and independent of v	_	May approach 60/n mV at low v but increase as v increases
	Constant	Constant	Virtually independent of v
	Equals 1and independent of v	no current on the reverse side	Equals 1 only for $\alpha = 0.5$

1.3.2. Square wave voltammetry

Square wave voltammetry (SWV) is a further improvement of staircase voltammetry, which is itself a derivative of linear sweep voltammetry. In linear sweep voltammetry the current at a working electrode is measured while the potential between the working electrode and the reference electrode is swept linearly with time.

Oxidation or reduction of species is recorded as a peak or trough in the current signal at the potential window. The potential waveform composed of a symmetrical square wave of constant amplitude is superimposed on a base potential staircase sweep [34,35] as illustrated in figure 1.5. The current is measured at the end of each wave just prior to potential change. The differential current is then plotted as a function of potential.

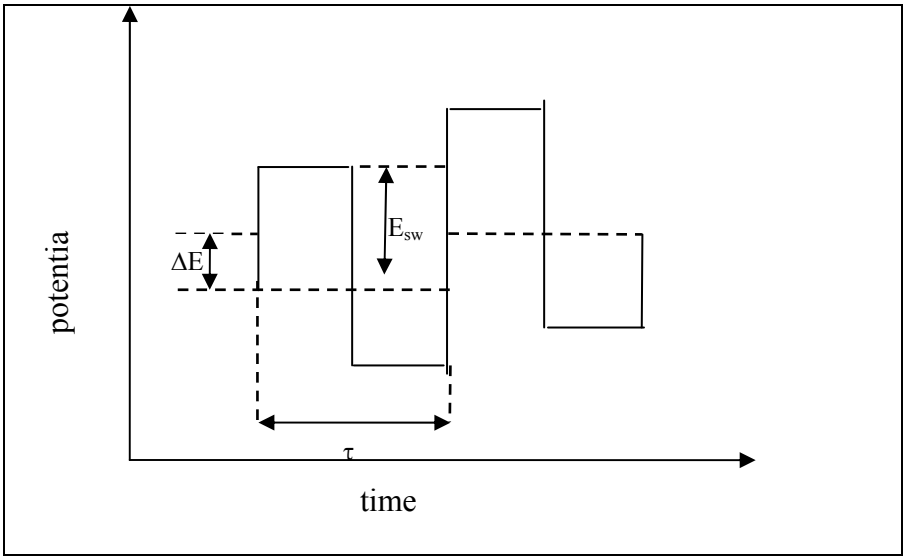

Figure 1.5: Square wave waveform potential sweep.

The excitation signal in SWV consists of a symmetrical square wave pulse of amplitude E_{sw} superimposed on a staircase waveform of step height ΔE, where the forward pulse of the square wave coincides with the staircase step. The net current, i_{net}, is obtained by taking the difference between the forward and reverse currents ($i_{for} - i_{rev}$) and is centered on the redox potential. This speed, coupled with computer

control and signal averaging, allows for experiments to be performed repetitively and increases the signal-to-noise ratio.

In this technique, a peak is a square wave which occurs at the $E_{1/2}$ of the redox couple because the current function is symmetrical around that potential [36,37]. Square wave voltammetry has several advantages, among these are its speed and excellent sensitivity partly because of its ability to discriminate against charging current [38-39] or to separate a capacitive current from a so called pseudocapacitance [40]. The peak height is directly proportional to the concentration of the electroactive species and direct detection limit as low as 10^{-8} mol.L^{-1} is possible. This technique includes the use of faster scan rates compared to conventional differential pulse voltammetry. Applications of square-wave voltammetry include the study of electrode kinetics with regard to catalytic homogeneous chemical reactions, determination of some species at trace levels. In this research, a computer-controlled square wave voltammetry was employed.

1.3.3. Chronoamperometry

Chronoamperometry belongs to the family of step techniques [41-44], which is a potential-controlled technique where the basis is the measure of current response to an applied potential as a function of time. If the potential is stepped from E_1, where no current flows

(i.e., the oxidation or reduction of the electrochemically active species does not take place) to E_2 where the current belongs to the electrode reaction, is limited by diffusion. The current flows at any time after the application of the potential step, (figure 1.6(a)). As with all step techniques, this one however, generates high charging currents which decay exponentially with time. It is most commonly investigated with a three electrode system. The resulting current-time dependence is monitored (figure 1.6(b)).

The current-time curve reflects the change in the concentration gradient in the vicinity of the surface which involves gradual expansion of the diffusion layer associated with the depletion of the reactant, thus the slope of the concentration profile decreases as time progresses. Accordingly, the current decays with time as given by the Cottrell equation, (equation 1.8).

$$I = \frac{nFAD^{1/2}C}{\pi^{1/2}t^{1/2}} \qquad (1.8)$$

where n, F, A, D, C, and t are number of electrons, Faraday constant, the surface area of the electrode, the diffusion coefficient, the concentration of analyte and time, respectively.

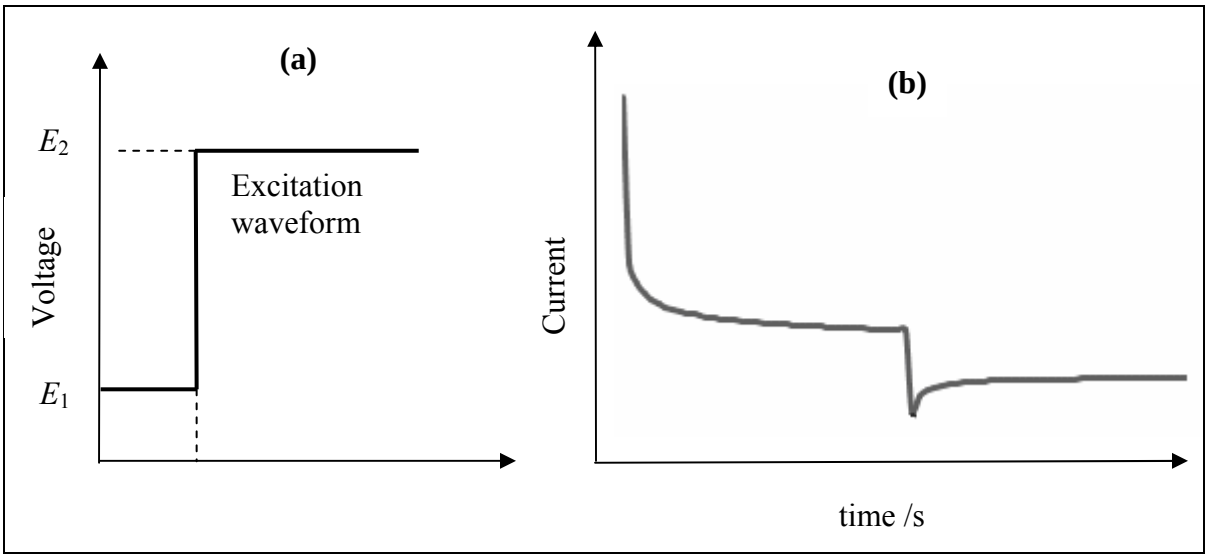

Figure 1.6 (a) Waveform of the potential step and (b) Chronoamperometric response.

1.3.4. Linear sweep voltammetry

Linear sweep voltammetry (LSV) is a method where the electrode potential is varied linearly with time with the scan rate ν = dE/dt and current versus potential is recorded. In LSV essentially only the first half-cycle of a cyclic voltammogram is executed and the rotating disk electrode is used in this experiment.

The rotating disk electrode is rotated in the solution under study and the current depends on the solution flow rate. For the rotating disk electrode, the time dependence is in the rotation rate of the disk, which in turn controls the solution velocity near the electrode. The rate of mass transport at the rotating disk electrode is varied by altering

the disk rotation speed [45]. The rotating electrode is mounted vertically to a controllable-speed motor and rotated with constant angular velocity. The components of the fluid velocity depends on this angular velocity of the disk, which is given by $\omega = 2\pi f$, where f is the rotation speed in revolutions per minutes (rpm) or rotation frequency in hertz. It depends on other factors such as the radial distance from the center of the disk (r), the coefficient of kinematic viscosity of the fluid (γ) and on the axial distance from the surface of the disk [46].

The diffusion-limited current at the rotating disk electrode is given by the Levich [47] equation based totally on mass-transfer limited conditions. The disk current I_k in the absence of diffusion control, that is, solely in the case of electron transfer controlled process is given by

$$I_k = FAK(E)C \tag{1.9}$$

with the surface area A of the electrode, the catalytic rate constant k as a function of the electrode potential E and the concentration C. A general equation of the disk current, taking into account both mass transport and electron transfer kinetics can thus be given as the Koutečky-Levich [48] equation:

$$\frac{1}{I} = \frac{1}{I_k} + \frac{1}{I_{\lim}} = \frac{1}{I_k} + \frac{1}{0.62nFAD^{\frac{2}{3}}\omega^{\frac{1}{2}}\gamma^{\frac{1}{6}}} \tag{1.10}$$

where I is the measured current, I_k and $I_{\lim}$ are the kinetic and diffusion-limited currents, respectively, n is the number of electrons transferred per molecule, F is the Faraday constant, A is the geometric electrode area, D is the diffusion coefficient ω is the rotation rate in rad.s^{-1}, and γ is the kinematic viscosity of the solution.

1.4. Chemically modified electrodes

A chemically modified electrode (CME) is an electrode surface coated with a thin film of selected conducting materials for the purpose of improving the chemical, electrochemical, optical, electrical and electron transfer properties of the film in a rational, chemically designed manner [49]. The modified electrode can thereby exhibit properties related to those of the modifying substance, e.g., electron-transfer mediation; acceleration or inhibition of electrode reactions; chemical, electrostatic, or steric selectivity; photosensitivity; and so on. Such method of construction which involves incorporating an electroactive substance onto a solid surface such as gold [50], carbon paste matrix [51], glassy carbon [52], pyrolytic graphite electrodes [53] has been applied until recently for a number of purposes such as the determination of trace amounts of some substances [54,55], electrocatalysis [56,57] and electrochemical sensors for the analysis of biologically important compounds [58]. CMEs may contain more than one modifying substance or more than one layer.

1.4.1. Methods of modifying electrode surface

A number of methods have been used to fabricate chemically modified electrodes. Such methods occur as a results of attaching molecules of modifying species by valence forces, covalent bonding,

coating by polymer (organic) or inorganic polynuclear, mixed films such as composites, hybrid organic-inorganic, or by mixing the modifier with electrode matrix material [58]. Several types of ring-substituted and unsubstituted MPcs and other organometallic complexes have been employed in the construction of electrochemical sensors using methods which do not require special equipment.

Confinement of these catalysts to the electrode surface is clearly advantageous from economic standpoint and improves the flexibility of the system by providing an option for reagentless sensing, stability and well-defined or sizeable electrochemical responses. Fabrication techniques of electroactive materials on conductive solid substrates that have attracted attention of researchers are described below.

1.4.1.1 Self-Assembly/chemisorption

The formation of self-assembled monolayers (SAMs) has attracted considerable attention since the late 1980s because of its potential use in many scientific and technological applications such as chemical sensors, biosensors and information storage devices [59]. SAMs provides means to controlling the chemical nature of the electrode-solution interface [60].

Spontaneous, chemically adsorbed monolayers of alkanethiols on gold substrate is based on the strong interaction between gold and

sulphur which are well suited for controlling and manipulating the reactivity at the interface. The thiol molecules adsorb readily from solution onto the gold, creating a dense monolayer with the tail group pointing outwards from the surface. If the molecule does not contain sulphur, for example carboxylated SWCNT, the use of a different substrate like silicon [61] can be used. One of the simplest ways of forming these ultrathin films is by mere immersion of the noble metal surface in a dilute millimolar solution of organic molecule for a specified time [62]. It is also possible to chemically functionalize the tail groups by performing reactions after assembly of the thiol SAM. The Au-thiolate bond is a strong, homolytic bond strength of 44 kcal/mol [63,64]. These alkanethiols are known to form densely packed crystalline or liquid crystalline material on gold with attractive Van der Waal forces between the alkyl chains that enhances the stability and order of the SAMs. The latter forces add up to strength for alkyl chains and plays an important role in aligning the alkyl chains parallel to each other. Such a self-assembly process results in a well organized and stable monolayers with hydrocarbon tails packed parallel to each other, tilted slightly relative to the substrate. The packing and order of monolayers are influenced by factors such as chain length, head group, solvent, immersion time and substrate morphology.

Research has shown that SAMs formed with longer alkane thiol chain lengths of carbon atom greater than 10, favour a more ordered packing and higher monomer density [59,61]. Electron transfer kinetics is also dependent on the carbon chain length of thiol molecules. Griveau and co-workers [65] reported that electrodes modified with thiols like cysteine, glutathione and 2-mercapoethanol are not stable over long period of time associated with the loss of the catalyst from the surface linked to passivation complications that are endemic to organosulphur compounds. To overcome this problem the use of SAM comes as an advantage where straight alkanethiol chain and macrocyclic complexes such as phthalocyanines or nanomaterials such as carbon nanotubes can be attached and form conductive and stable films.

The structure in Figure 1.7(a) could arise, for example, with an assembly in which the substrate imposes a head-group spacing leading to lower density than a closest packed arrangement. Generally, the greater the mismatch between the van der Waals radii of the tail groups and the head groups and between these quantities and the substrate lattice parameters, the greater the tendency for the monolayer to deviate from well-arranged structures such as in Figures l.7(b) and l.7(c) and to exhibit structural disorder and defects.

In this case, a final structure could arise as a compromise between a tendency for tails to pack parallel to one another and be oriented perpendicular to the surface (in order to maximize interlocking interactions of CH_2 groups in an alkyl chain) and a tendency for the head groups to maintain an open structure for which parallel, tilted tails (i.e figure 1.7(b)) do not pack optimally.

The word SAM, simple mean a monomolecular thin film of organic compound on flat conducting metal. Cyclic voltammetry and impedance spectroscopy are important techniques which provide useful information about redox properties of attached groups, distribution of defects like pinholes, kinetics and mechanism of monolayer formation.

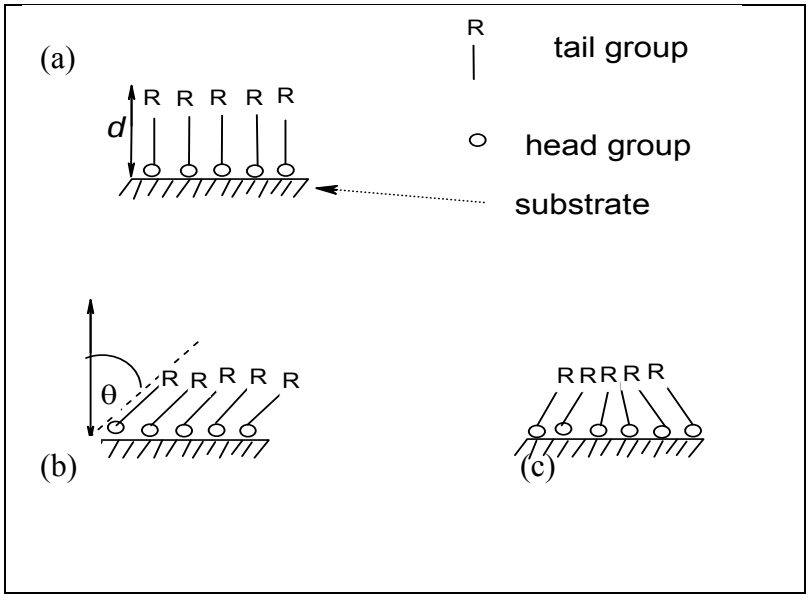

Figure 1.7: Models of an organized monolayer.

The redox activity of the SAM is obtained by using an external redox probe and voltammetry can provide additional information about the mode of surface confinement. One advantage of using SAM modified electrodes is that they are very stable and can form a highly ordered ultrathin films on solid surfaces [66]

Self-assembly can be devided into four main types. *Static*, *dynamic*, *biological* and *templated* self-assembly [67] Systems that are at global equilibrium and do not give off energy, for example molecular crystals [68,69] and globular proteins, are formed by static self-assembly.

Alkanethiol monolayers can also be assembled on gold nanoparticles confined to indium tin oxide. Alternatively, mixing two different hydrocarbons which are carboxyl group terminated in the preparation solution, the mixed SAMs can be prepared. The relative proportion of the two functionalities in the assembled SAM will then depend upon several parameters, like the mixing ratio in solution, the solubilities of the hydrocarbon in the solvent used, and the properties of the terminating groups. The main focus in this work was on the mixture of ferrocenes and carbon nanotubes, since they both contain the same carboxyl functional groups.

Although SAMs are stable in a wide range of potential, the layer is desorbed from the surface at very cathodic potentials [70]. Wang *et*

al. [71] has reported that carboxylic acid, (COOH) and amine (NH_2) terminated SAMs are used to mimic negatively and positively charged surfaces, respectively.

1.4.1.1.1 Characterization of SAM-modified electrodes

A list of non-electrochemical analytical methods for characterisation of SAM-modified electrodes includes infra red spectroscopy, X-ray photoelectron spectroscopy and scanning probe microscopy. Electrochemical techniques especially, cyclic voltammetry (CV) [72,73], have proven to be effective for SAM characterisation. Other methods can be used for the determination of surface concentration, electron-transfer kinetics, sensitivity and electrode's limit of detection, such as the method used in this work, namely impedance spectroscopy and chronoamperometry.

The surface roughness of gold electrode surface plays a crucial role in determining whether or not the SAMs formed will have pinholes and defects or not. Increase in surface roughness usually increases the chances of having pinholes and defects because it leads to formation of SAMs with poor uniformity [74-77].

It has been reported that an MPc species that is surface confined with flat orientation has a surface coverage concentration of approximately 10^{-10} mol cm^{-2}, free of pinholes and defects. Nirmalya *et*

al. [78] reported that if a decrease by one order of magnitude in double layer capacitance is observed, confirms SAM formation on the solid surface while lack of redox behaviour indicates surface passivation.

1.4.1.1.2 Application of SAM modified electrodes

Self-assembly technique offers several number of advantages over other film formation techniques. These advantages include spontaneous adsorption to the electrode surface, resulting in thermodynamically equilibrated thin film structures. Despite the popularity of the MPcs as efficient electrocatalysts for analysis of a variety of molecules, their use as electroactive SAMs still remain largely unexplored. However, considerable interest has been placed on SAMs of organothiol on gold surfaces. Analytical application of these SAMs is the fabrication of a number of biosensors and immunosensors [79], enzyme biosensors [80], DNA hybridization biosensors [81] and metal ion sensors [82]. The fundamental application of SAM modified electrodes is used in the study of heterogeneous electron transfer [83,84].

1.4.1.2 Electrodeposition

This is a process used in electroplating in which the current is used to reduce cations of a desired material from a solution and coat a conductive metal with a thin layer of the material. To acquire this, the electrode is immersed in an electrolyte solution containing one or more dissolved salts as well as other ions that permit the flow of electricity, followed by repetitive voltammetric scanning within a specified potential window [85].

1.4.1.3 Drop-dry method

This method involves drop-coating the electrode with small droplets of the desired solution of volatile solvent such as dimethylformamide and then allowed to dry out [87-89]. The films prepared in this way are usually non-uniform. However, the morphology of the film depends on the concentration of the casting solution, rate of solvent evaporation, nature of the solvent and the roughness of the electrode surface.

1.4.1.4. Dip-dry coating

Dip-dry coating involves immersion of the electrode in a solution for a period sufficient for spontaneous film formation to occur by adsorption. Then the electrode is withdrawn from the solution and the solvent is allowed to dry out [90,91].

1.4.1.5 Spin coating

Spin-coating also known as spin casting is a procedure in which the excess amount of a solution is placed on the substrate and rotated at high speed in order to spread the fluid by centrifugal force. Rotation is continued while the fluid spins off the edges of the substrate, until the desired thickness of the film is achieved. The solvent used is usually volatile and simultaneously evaporates. As a result, the higher the angular speed of spinning, the thinner the film. However, the thickness of the film depends on the concentration of the solution and the solvent. Spin coating is widely used in microfabrication and photolithography and the film may show lower percentage coverage of crystallites than a simple evaporated film [92,93].

1.4.1.6 Vapour deposition

This process is also known as the chemical vapour deposition (CVD). It is used to produce high-purity and high performance thin films. In a typical CVD process the substrate is exposed to one or more volatile precursors which react and decompose on the substrate surface to produce the desired deposit.

1.4.1.7 Langmuir-Blodgett

In 1930, Langmuir and blodgett invented the technique that involves forming an ordered monolayer or multilayer films at the air-water interface and then transfer the film to the electrode surface by immersing the solid substrate into or from the liquid. A monolayer is added with each immersion step thus films with accurate thickness can be formed and can be repeated with several layers, if desired, of different properties [94].

1.4.1.8 Electropolymerisation

In this method the electrode is immersed in an approximately 1 mM concentrated solution of the modifier followed by repetitive voltammetric scanning within a specified potential window. The resulting voltammogram of the first scan is different from the

subsequent scans indicative of the formation of the new species on the electrode surface. Li and Guarr [95] reported that very thin films of cobalt and nickel phthlocyanine complexes can be easily prepare using electropolymerization method and the polymeric coating produced exhibit electronic conductivity over a wide potential range. Kang *et al*. [86] developed a potentiometric pH sensor prepared by electropolymerization of a number of monomers on glassy carbon electrode.

1.5. Organo-iron complexes and carbon nanotubes

1.5.1. Metallophthalocyanine modified electrodes

Phthalocyanine was discovered during the industrial production of phthalimide at the Grangemouth plant, Scottish Dye Ltd in 1928 [96,97]. Phthalocyanine (Pc) complex (Figure 1.8) is a macrocyclic compound having an alternating nitrogen carbon atom ring structure and has been the most studied classes of organic functional materials. The diverse functionality of this macrocyle originates from its 18 π-electron aromatic system which closely resembles the naturally occuring porphyrin systems. Recently, More than seventy MPc complexes are known [98].

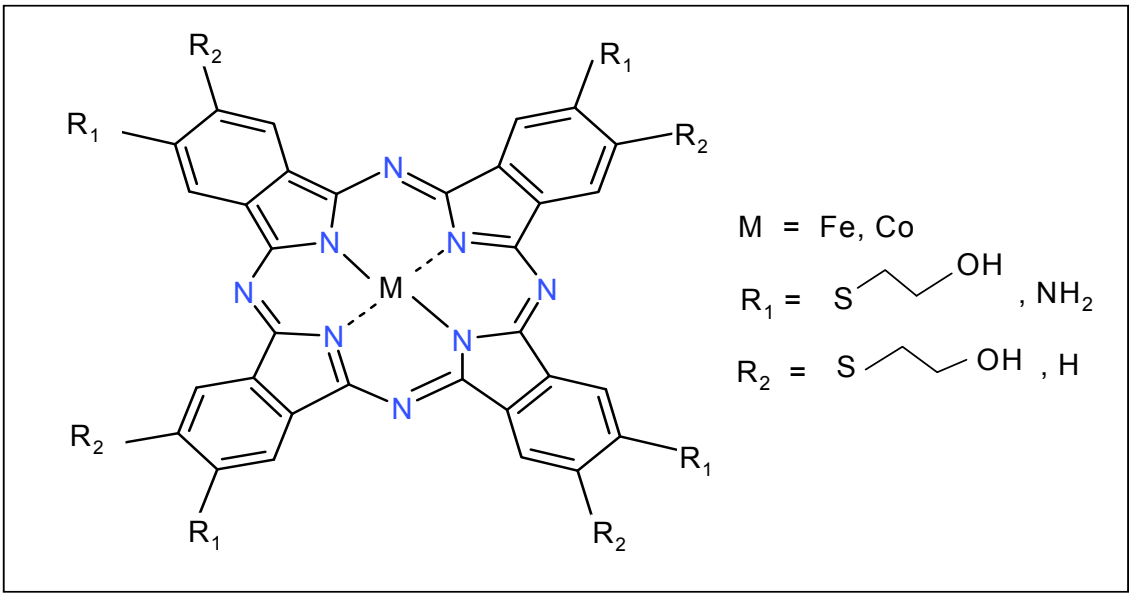

Figure 1.8: Geometric structure of metallophthalocyanines.

Like the porphyrins, the Pc macrocycle can play host to a number of different metal ions in its central cavity by coordinate bonds with the four isoindole subunits linked together by aza nitrogen atoms [98] to form metallophthalocyanines (MPcs). Incorporation of different ring substituents in the peripheral and non peripheral positions is also possible. The central atoms of MPc can carry additional ligands.

The name, Phthalocyanine, was conceived in the 1900's as a combination of prefix *phthal*, originally from the greek word naphtha meaning rock oil and *cyanine* is a synthetic dye. Many of Pc properties, for example, solubility can be varied by changing the central metal ions, axial ligands and ring substituents [99,100].

Phthalocyanines are beautiful bright blue to green coloured [99,100] that have found applications in almost every area of modern science and technology. Their bright colours have found extensive use as colorant in various areas of spin dyeing, textile dyeing and paper industry [97]. More recently they have been employed in several applications such as the photoconducting material in laser printers [97,101] and the light absorbing layer in re-writable compact disks [102-104]. They are also used as photosensitisers in laser cancer therapy [105-109], as nonlinear optical materials and as industrial catalysts, fuel cells [110] and electrochemical sensors [111-113].

MPc complexes have also established themselves as powerful electrocatalysts [102-104] when used to modify electrode materials for developing electrocatalysts and electrochemical sensors for different potential technologically important applications [114,115]. MPc complexes are readily available since they are relatively easier to synthesize and are produced in large amounts for industrial applications, less expensive and more stable to degradation than the porphyrin complexes. In this work, metallophthalocyanine together with single-walled carbon nanotubes are used as modifier in the SAM formation for detections of biological substances such as thiocynate, epinephrine and dopamine. In this work, FePc complexes were studied with a view to establish their SAM properties.

1.5.2. General overview on ferrocene-derivatised self-assembled monolayers

Ferrocene is the organometallic compound, a prototypical metallocene compound consisting of two cyclopentadienyl rings bound on opposite sides of the central metal with the five carbon atoms of each ring forming a pentahapto (η^5) arrangement (Figure 1.9).

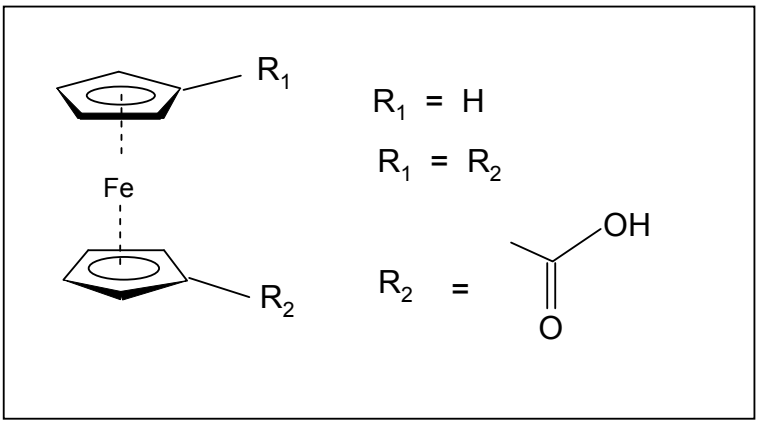

Figure 1.9: The structure of ferrocenemonocarboxylic acid (FMCA) and ferrocenedicarboxylic acid (FDCA). Both FMCA and FDCA were studied in this work.

Ferrocene undergoes a one-electron oxidation at a low potential and substituents on the cyclopentadienyl ligands alters the redox potential as expected. Electron-withdrawing groups, such as carboxylic acid, shift the potential in the anodic direction (more positive). Ferrocene and its derivatives are antiknock agents used in fuel for petrol engines and are safer than tetraethyl lead which was used previously [116]. It has no large scale applications but has found broad applications as outer sphere redox mediators, ligand scaffolds and phamarceutical candidates which exhibit anticancer activity [116]. Electron properties of a series of ester-protected amino acids coupled to ferrocenecarboxylic acid were studied by Kraatz *et al*. [117] and they showed that the redox potential of the ferrocenyl group is

influenced by the amino acid substituents [118]. Ferrocene can be used to deposit certain kind of fullerenes, especially carbon nanotubes. Many organic reactions can be used to modify ferrocenes, and in this work ferrocenemonocarboxylic acid and ferrocenedicarboxylic acid were used as a mixture with carboxylated carbon nanotubes immobilized on gold surface via self-assembly technique, to investigate their joint electrochemical behavior.

1.5.3. Introduction to carbon nanotubes

Cage-like fullerenes molecules were discovered by a team headed by Harry Kroto [119], in 1985. In 1990, a team at the Max Plank institute showed that fullerenes could be mass-produced by passing a spark of electric current between two touching graphite electrodes surrounded by helium. The heat produced vaporizes the graphite and fullerenes form as the gaseous carbon cools. Iijima [1], who was then studying carbon-nanofibre and its production, which uses similar method, but decided to keep the two electrodes a short distance apart. To his surprise, he found carbon needle-like material growing on the negative electrode. It was carbon nanotubes. The introduction of catalytic plasma-enhanced chemical vapor deposition (C-PECVD) in the 1900s provided additional control mechanism over the growth of carbon nanostructures.

CNTs are divided into two main types. Figure 1.10 shows the distinct two types of carbon nanotubes. Single-walled nanotubes (SWCNTs) consist of a single graphite sheet seamlessly wrapped into a cylindrical tube that run the full length of the nanostructure. Malechko *et al.* [2] made a clear distinguishing characteristic between nanotubes and nanofibres in terms of the different chemical properties since defect-free nanotube walls do not contain the exposed edges and unsaturated bonds of graphene planes, and therefore makes the nanofibers to be more reactive than nanotubes.

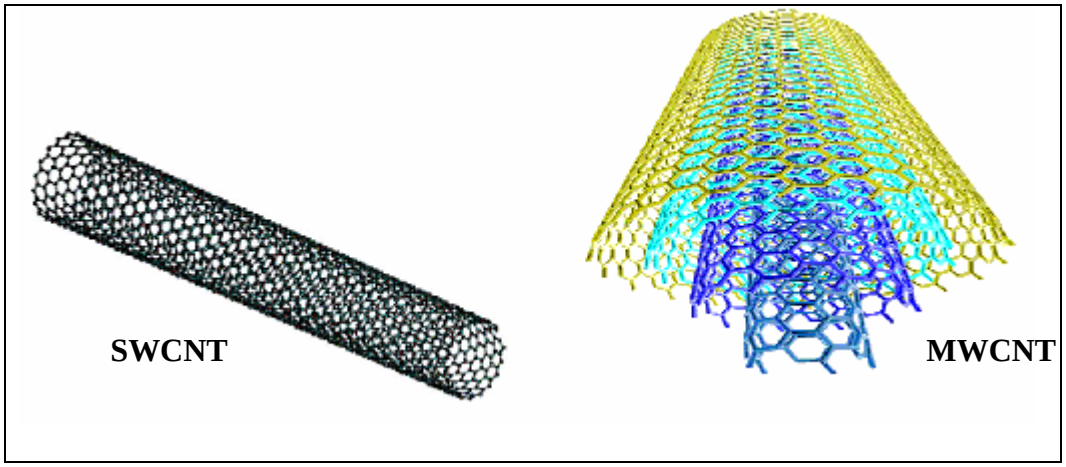

Figure 1.10: Graphical representation of SWCNT and MWCNT.

To expose the defect sites of nanotube, the harsh acid treatment of these materials was done in this work. Multiwalled nanotubes (MWCNTs) comprise an array of such nanotubes that are concentrically nested like rings of a tree trunk. Nanotube diameters range from ~0.4

to >3 nm for SWCNTs and from ~1.4 to at least 100 nm for MWCNTs [2,120]. CNTs form the basis for nanoscale tweezers that can pick-up and move tiny particles [121,122]. SWCNTs and MWCNTs are usually made by carbon-arc discharge, laser ablation of carbon, or chemical vapor deposition [120]. Synthesis of boron and/or nitrogen substituted nanotubes is one possible method to control the electronic properties of nanotubes [123-125].

However, it has been a practical problem to control the size and length of these synthesized nanomaterials, which seriously restrict the future applications. Lai *et al*. [126] was able to synthesize carbon nitride nanotubes (CN-NT) using an electron cyclotron resonance chemical vapor deposition (ECR–CVD) system with a mixture of C_2H_2 and N_2 as precursors without using any catalyst. Nanotube properties can thus be tuned by changing the diameter. Unfortunately, SWCNTs are presently produced only on a small scale and are extremely expensive in their purest form.

All currently known synthesis method for SWCNTs result in major concentration of impurities. Carbon-coated metal catalyst contaminates the nanotubes of the HiPco route, and both carbon-coated metal catalyst and, typically, ~60% forms of carbon other than nanotubes are formed in the carbon-arc route [127,128]. These

impurities are typically removed by acid treatment, which introduces other impurities, can degrade or shorten nanotube length and perfection, and adds to nanotube cost. Nevertheless, the acid treatment was used in this project to shorten the tubes and introduce the carboxyl groups for ease of attachment for SAM formation. Vertically aligned periodic arrays of carbon nanotubes (CNTs) are used to create topographically enhanced light-trapping photovoltaic cells [129].

1.6. Physico-chemical characterization of modified electrodes

1.6.1. Electrochemical Impedance Spectroscopy (EIS)

The development of solid state batteries as rechargeable high-power-density energy storage devices were since developed in the late years of World War II. As a result, the characterization of systems with solid-liquid interfaces is the new revolution in high-temperature electrochemical sensors in environment, industrial, energy efficiency control and the introduction of fuel cells. Electrochemical impedance spectroscopy is a newest and powerful tool for characterization of electrochemical system mainly focusing on the electrical properties of materials and their interfaces with electronic conducting electrodes [130].

Electrochemical impedance spectroscopy describes the measurement of the impedance of a system as a function of frequency of an applied perturbation.

1.6.1.1 Basics of electrochemical impedance spectroscopy

Impedance is a measure of opposition to a sinusoidal alternating current (AC). From a physical point of view, impedance is just a totally

complex resistance (measured in Ohms, Ω) that appears when an AC current flows through a circuit made of resistors, capacitors, inductors or any combination of these. This magnitude shows a complex notation, with a resistive or real part attributable to resistors (in phase with the applied voltage) and a reactive or imaginary part attributable to the contribution of capacitors (out of phase with the applied voltage by $+\pi/2$) or inductors (out of phase with the applied voltage by $-\pi/2$) as shown in figure 1.11(a).

The graphical or vector representation of imaginary impedance against the real impedance showing how impedance, Z, and phase angle, ϕ, are defined, and is called the impedance plot as illustrated in figure 1.11(b). When working with electrochemical systems, this perturbation is normally an AC voltage of small amplitude, typically 5–10 mV peak-to-peak, and the response is a current that differs in amplitude and phase (phase difference, ϕ) with the applied voltage.

Impedance is a complex function, therefore, the total impedance consist of the real component (Z') located on the abscissa which is the resistance and the imaginary component (Z'') which is the reactance, locate on the ordinates of the impedance plot in figure 1.11(b).

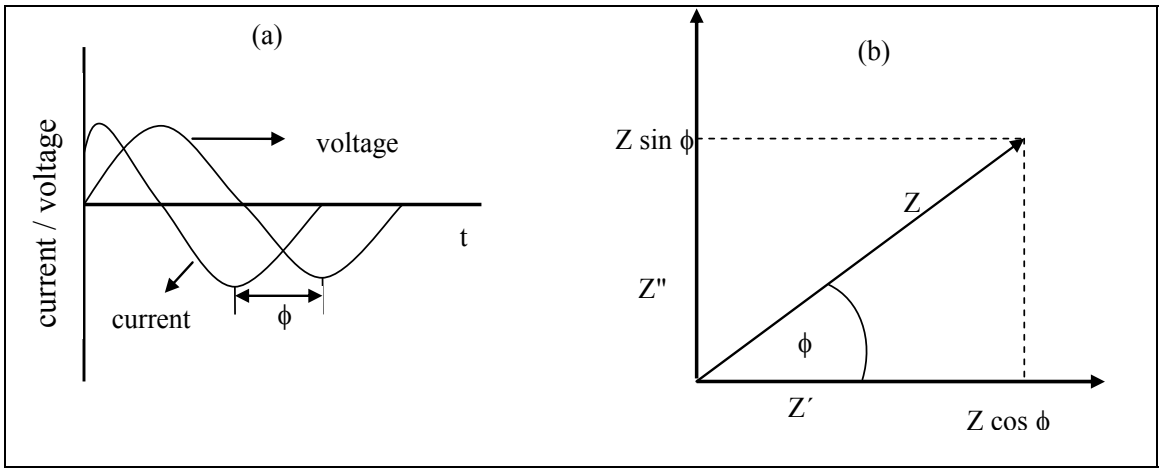

Figure 1.11: (a) Applied voltage and (b) resulting current response.

Impedance Z, Z" and Z˙ are related as follows :

$$Z = Z' + jZ'' \qquad (1.11)$$

where the complex number j is $(-1)^{1/2}$. In terms of the resistance and reactance, equation 1.11 can be expressed as :

$$R - jX \text{ ; and } X = 1/\omega C \qquad (1.12)$$

where R is the resistance (measured in Ω), X the reactance, C the capacitance (measured in Farads, F), and ω the applied angular frequency (measured in rad.s^{-1}; $\omega = 2\pi f$, f is the frequency measured in hertz). The ratio of applied voltage to measured current is the impedance, Z of the system, described by Ohms law, equation 1.13:

$$Z = E/I \qquad (1.13)$$

where E is the potential voltage or energy in volts and I the current in amperes. Impedance is, in simple terms, applying a constant voltage

across a resistance R which induces a constant current I. Impedance parameters are measured as a function of frequency of the applied perturbation.

1.6.1.2 Applications and data representation

A common way of showing the resulting data is the complex plane or Nyquist Plot (Figure 1.12), in which the real Z´ versus the imaginary Z" components of the impedance are plotted.

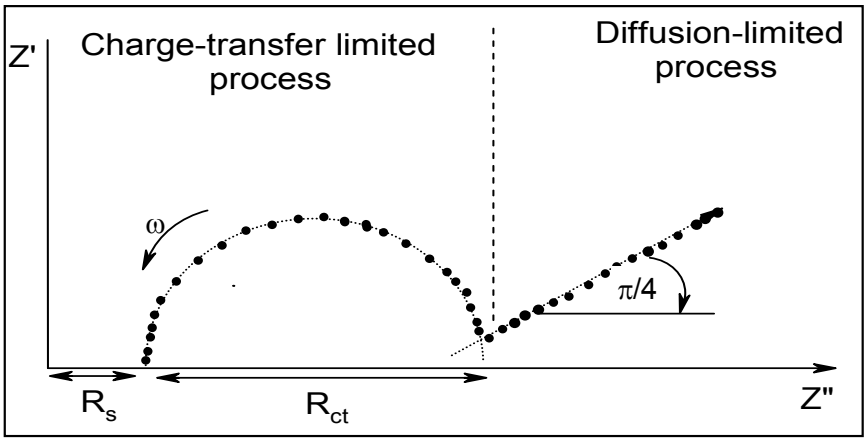

Figure 1.12: Nyquist plot for the electrochemical system with diffusion and kinetics limited processes.

In this plot, two separate processes are very well differentiated, that is, a semicircle relating to a charge-transfer-controlled process, the intercept of which with the x-axis gives R_s and R_{ct} values, and a straight line with a slope of 1 due to Z_w, whose extrapolation to the x-

axis allows calculation of the Warburg coefficient, σ , from which the diffusion coefficients of the electroactive species can be estimated using equation 1.14 [131].

$$\sigma = \frac{\sqrt{2}\left(RT / F\right)}{FAC\sqrt{D}} \qquad (1.14)$$

were F is the Faraday's constant, R is the gas constant, T is the temperature and A the geometric area of the electrode. From the frequency at the top of the semicircle, where Z" is maximum, the time-relaxation constant, τ, for the Faradaic process can also be calculated.

Another way of presenting impedance data is the Bode Plot (figure 1.13) which gives an indication of the frequency where the impedance was measured. Bode data representation is the plot of logarithm of the absolute value of Z and the phase angle, ϕ, plotted against the logarithm of frequency *f*. These data presentations give direct information about f and ϕ that help ascertain the different constituent phases of the system more easily. Thus, in those frequency regions where a resistive behaviour is dominant, a horizontal line is observed for the log Z vs log *f* representation and a ϕ close to 0^{o} is measured. Also, capacitive behaviour within a frequency region is described by a straight line with a slope of -1 in the log Z vs log *f* plots and a ϕ around 90^{o}, whereas diffusion-controlled

phenomena (Warburg Impedance) would give a straight line with a slope of -1/2 and a ϕ of 45°. A detailed mathematical description of all the above parameters can be found elsewhere [132,133].

To establish whether the experimental impedance data (Nyquist and Bode plots) can be fitted to any equivalent circuit, the spectrum should be first subjected to the so-called Kramers-Kronig (K-K) assumption.

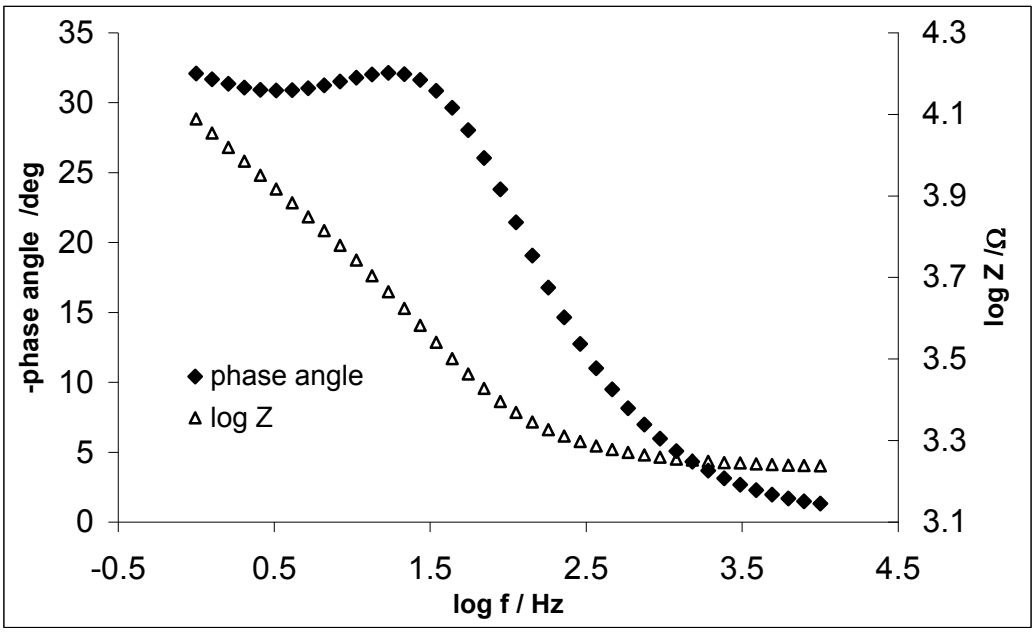

Figure 1.13: Typical Bode plots indicating the phase angle and logarithm of impedance versus frequency.

The main essence of the K-K test is simply to check whether the measured impedance spectra comply with the assumptions of the well known K-K transformation, which are (i) that the impedimetric

response is only related to the excitation signal; (ii) that the impedimetric response is linear (or the perturbation is small, e.g., <10 mV, for non-linear systems; (iii) that the system does not change with time, say due to ageing, temperature changes, non-equilibrium conditions, etc; and (iv) that the system is finite for all values of ω, including zero and infinity [132,133]. Failure of the K-K test, signified by a large value of pseudo χ^2 is usually an indication that no good fit can be obtained using the electrical equivalent circuit methods. It should be noted that aside from visual inspection of goodness of the fitting lines, two accurate ways to establish how well the modeling functions reproduce the experimental data sets are the relative error estimates (in %) and chi-square functions (χ^2) [134], which is the sum of squares of the relative residuals (i.e., sum of the real and imaginary χ^2), easily obtained from the K-K test.

Experimental impedance data of an electrochemical cell can be easily fitted to the impedance of an equivalent circuit mainly comprising resistors and capacitors. Equivalent circuit concept is the heart of impedance analysis. In such circuits, a resistance ideally describes a conductive path, such as that generated by the bulk conductivity of the system or the charge-transfer step due to an electrode reaction, whereas a capacitance generally describes space-charge-polarisation regions within the system as well as modification

of an electrode surface due to adsorption processes or polymer-layer deposition. The Randles circuit [135] in Figure 1.14, is the simplest equivalent circuit that describes an electrochemical cell where a single-step Faradaic process in the presence of diffusion may occur.

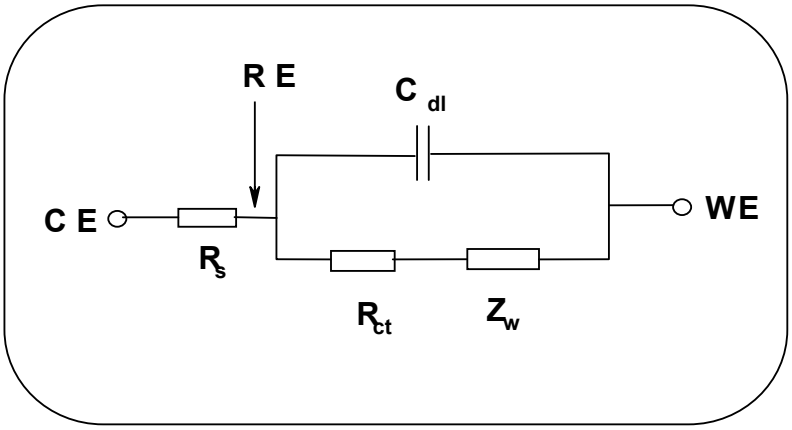

Figure 1.14: Randles electronic equivalent circuit (for an ideal situation).

It combines three components, namely the electrolyte resistance between working and reference electrodes R_s, the double layer capacitance (C_{dl}), and the Faradaic impedance consisting of charge-transfer resistance R_{ct} at the working electrode-electrolyte interface and the so-called Warburg Impedance Z_w, which reflects the influence of the mass transport of the electroactive species on the total impedance of the electrochemical cell. Thus, for those diffusion-limited processes, Z_w becomes dominant, whereas for those charge-transfer-controlled processes, only R_{ct} can be obtained.

For a practical situation, the double layer capacitance (C_{dl}) in the Randles equivalent electric circuit is replaced by the constant phase element (CPE) as depicted in Figure 1.15.

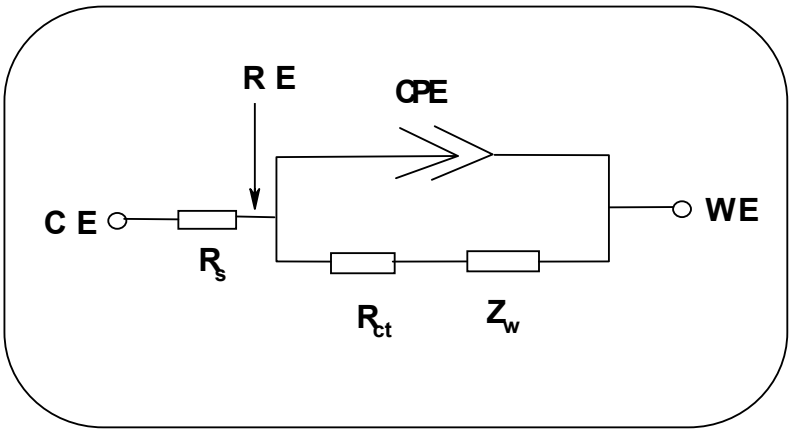

Figure 1.15: Modified Randles equivalent electric citcuit (for a real practical situation)

The impedance of the CPE (Z_{CPE}) is a power-law dependent interfacial capacity defined as [136]:

$$Z_{CPE} = \frac{1}{[Q(j\omega)^n]} \qquad (1.15)$$

where Q is the frequency-independent constant relating to the surface electroactive properties, ω is the radial frequency, the exponent n arises from the slope and the exponent n has values $-1 \leq n \leq 1$ which is estimated from the slope of log Z vs log f. If $n = 0$, the CPE behaves as a pure resistor; $n = 1$, CPE behaves as a pure capacitor, $n = -1$ CPE behaves as an inductor; while $n = 0.5$ corresponds to Warburg

impedance (Z_w) which is associated with the domain of mass transport control arising from the diffusion of ions to and from the electrode|solution interface. Generally speaking, CPE has been known to occur via several factors notably (i) the nature of the electrode (e.g., roughness and polycrystallinity), (ii) distribution of the relaxation times due to heterogeneities existing at the electrode/electrolyte interface, (iii) porosity and (iv) dynamic disorder associated with diffusion [137].

1.6.1.3 Factors affecting rate of electron transfer

Several factors affect the response of modified electrode, notably, the SAM-modified electrode. Passivation is one of them. It results if the electrode surface is modified with a resistive monolayer and hence alters their AC response. In terms of the Randles equivalent circuit, some components are affected [134]. Firstly, at high frequency where the electrode reaction is purely kinetic controlled, the heterogeneous charge-transfer resistance is expected to increase due to inhibition of the electron-transfer rate.

The increase in the charge-transfer resistance is related to the electrode coverage and is given by:

$$1 - \theta = \frac{R_{ct}^{0}}{R_{ct}} \qquad (1.16)$$

where θ is the apparent electrode coverage, assuming that all the current is passed via bare spots on the electrode, R_{ct}^{0} is the charge-transfer resistance measured at a bare electrode, and R_{ct} is the charge-transfer resistance measured under the same conditions at the monolayer-covered electrode.

Secondly, at lower frequencies the Warburg impedance is expected to deviate from a linear dependence upon $\omega^{1/2}$, which is the behaviour in the case of a semi-infinite diffusion. Such deviation would be manifested in cases where the defects or pinholes in the monolayer are far apart from each other when compared to the diffusion layer thickness. In this situation when the diffusion layers of neighbouring pinhole overlap. There maybe, however, a situation where the diffusion layers do overlap, even at highly covered electrodes. Then, the AC response at low frequencies resembles the behaviour of bare electrodes.

Equation 1.16 assumes that the current is due to the presence of defects within the monolayer [131] (defect is a site at which molecules or ions can approach the electrode surface at a distance shorter than the normal thickness of the SAM) and should not be used when the surface coverage values are close to 1, i.e $\theta > 0.9$. Using these θ values, the size and the distance between pinholes may be estimated

from equations (1.17) and (1.18). A pinhole is a site at which the electrode surface is exposed to the electrolyte.

$$r_a = \frac{r_b}{\sqrt{(1-\theta)}} \tag{1.17}$$

$$r_b = \frac{\gamma(1-\theta)}{\sigma\sqrt{\frac{0.72}{D}}} \tag{1.18}$$

where r_a and r_b are the size and distance between pinholes, respectively, γ is the y intercept of the plot of Z' vs $\omega^{-1/2}$. Graphical representation that illustrates the concept of defects and pinholes is shown in figure 1.16.

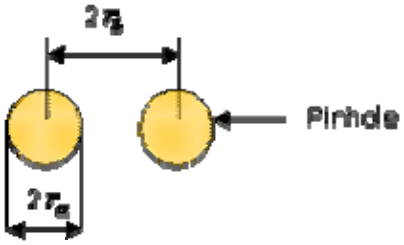

Figure 1.16: Illustration of the defects and the pinholes.

1.6.2. Atomic Force Microscopy

Scanning probe microscopes (SPM) describes a broad group of instruments use to image and measure properties of chemical species on solid surfaces. The two major forms of SPM are scanning tunneling

microscopy (STM) and atomic force miscroscopy (AFM). Acquiring a topographic image with high resolution to investigate the properties of a sample surface, atomic force miscroscopy, (AFM), is the standard technique to use.

Atomic force microscopy is a probe microscope which was invented in 1982 [138] and operates by measuring the force between the probe and the sample [139,140]. The probe consists of a sharp tip made of silicon or silicon nitride, attached to a force-sensitive cantilever. The tip scans across the surface by a piezoelectric scanner, and the cantilever deflects in response to force interactions between the tip and the substrate. Such deflection is monitored by bouncing a laser beam off it onto a photodector. The Atomic Force Microscope was developed to overcome a basic drawback with STM, that it can only image conducting or semiconducting surfaces or samples. The AFM, however, has the advantage of imaging almost any type of surface, including polymers, ceramics, composites, glass, and biological samples [141]

The atomic force microscope relies on the force between the tip and sample, knowing this force is important for proper imaging. Hook's law gives :

$$F = -kz \qquad (1.19)$$

where F is the force, k the stiffness of the lever, and z is the deflection of the cantilever. The force is not measured directly, but calculated by measuring the deflection of the lever, and knowing the stiffness of the cantilever. When the maximum deflection for a given force is needed, a soft spring is required. This makes the spring the critical component because a stiff spring with high resonant frequency is necessary in order to minimize the sensitivity to vibrational noise [141]. The resonant frequency of the spring is given by equation 1.20: [138]

$$f_o = \tfrac{1}{2}\pi\sqrt{k/m_o} \qquad (1.20)$$

where k is the spring constant and m_o is the effective mass that loads the spring. Equation 1.20 suggests that as k is reduced to soften the spring, m_o must also decrease to keep the ratio k/m_o large. Binning *et al*. [138] proposed a measurement of ultrasmall forces on particles as small as a single atom by monitoring the elastic deformation of different types of springs as a measure of force.

(a) Contact mode AFM

This is a scanning probe mode which operates by rastering a sharp tip across a sample. The performance of AFM is critically dependent upon the physical characteristics of the cantilever of low spring constant and the tip. A low interatomic force is maintained on

the cantilever as it rasters and thereby pushing the tip against the sample. The repulsive force between the tip and the sample or the actual tip deflection is recorded relative to spatial variation and then converted into an analogue image of the sample surface. The AFM tip is manually brought close to the sample surface and the scanner makes the final adjustment in tip sample distance based on the setpoints determined by the user. The tip in contact with the sample surface through any adsorbed gas layer is then scanned across the sample under the action of piezoelectric actuators by moving either the sample or the tip relative to the other. At the back of the cantilever is the laser beam which reflects off the cantilever surface to a split photodiode and then detects the small cantilever deflections.

(b) Non-contact mode

Non-contact mode AFM does not suffer from tip or sample degradation effects that are sometimes observed after taking numerous scans with contact AFM. This is due to the tip of the cantilever which does not come in contact with the sample surface. The cantilever is instead oscillated at a frequency slightly above its resonance frequency where the amplitude of oscillation is typically a few nanometers (<10 nm) [138]. This makes non-contact AFM preferable to contact AFM for measuring soft samples. In the case of rigid samples, contact and non-contact images may look similar.

However, if a few monolayers of adsorbed fluid are lying on the surface of a rigid sample, the images may look quite different. An AFM operating in contact mode will penetrate the liquid layer to image the underlying surface, whereas in non-contact mode an AFM will oscillate above the adsorbed fluid layer to image both the liquid and surface. However, both contact and non-contact mode AFM were used in this thesis.

1.6.3. Scanning Electron Microscopy

Scanning electron microscopy, SEM, is used for inspecting topographies of specimens at much greater resolution, approximately 5nm magnifications [142]. During this inspection, a beam of electrons is focused on a spot volume of the specimen, resulting in the transfer of energy to the spot. These bombarding electrons, also referred to as primary electrons, dislodge electrons from the specimen itself. The dislodged electrons, also known as secondary electrons, are attracted and collected by a positively biased grid or detector, and then translated into a signal. To produce the SEM image, the electron beam is swept across the area being inspected, producing many such signals. These signals are then amplified, analyzed, and translated into images of the topography being inspected.

The energy of the primary electrons determines the quantity of secondary electrons collected during inspection. The emission of secondary electrons from the specimen increases as the energy of the primary electron beam increases, until a certain limit is reached. Beyond this limit, the collected secondary electrons diminish as the energy of the primary beam is increased, because the primary beam is already activating electrons deep below the surface of the specimen. Electrons coming from such depths usually recombine before reaching the surface for emission.

A beam of electrons must travel to the sample, therefore, the sample must be vacuum compatible and either electrically conducting or coated with a conductive layer to avoid sample build-up [143]. The surface of a solid sample is scanned in a raster pattern with a beam of energetic electrons to produce signal of several types including backscattered, Auger electrons and X-ray fluorescence photons. Backscattered electrons serve as the basis of scanning electron microscopy, whereas, X-ray emission is used in electron microprobe analysis.

1.6.4. X-ray Photoelectron Spectroscopy

Electron spectroscopy is a powerful tool for the identification of most the elements in the periodic table with the exception of

hydrogen and helium. It provides useful information about the electronic structure of molecules, permits determination of the most oxidation state of an element and the type of species to which it is bound. For the study of surfaces, there are three types of electron spectroscopy. The most common type, which is based on upon irradiation of the sample surface with monochromatic X-radiation is called X-ray photoelectron spectroscopy (XPS).

It utilizes X-Rays with low energy (typically 1-2 keV) to knock off photoelectrons from atoms of the sample through the photoelectric effect. The energy content of these ejected electrons is then analyzed by a spectrometer to identify the elements where they came from [144]. The spectra provide not only qualitative information about the type of atoms present in a compound but also the relative number of each type. It is worthwhile pointing out that the photo-electrons produced in XPS are incapable of passing through a solid. Thus the most important application of electron spectroscopy is the accumulation of information about surfaces.

Its use includes identification of active sites and poisons on catalytic surfaces, determination of surface contaminants on semiconductors, analysis of the composition of human skin and the study of oxide surface layers on metals and alloys.

1.7. Background on the studied analytes

1.7.1. Potassium thiocyanate

Thiocyanate is considered to be non-toxic and its concentration in mining effluent is not regulated at the present time [145]. However, it is known that ultraviolet light decomposes thiocyanate to form cyanide, it is then possible that sunlight may liberate cyanide levels toxic to aquatic life from effluent rich in thiocyanate. In view of these considerations, it is not unlikely that in the future some limit may be imposed on the concentration of thiocyanate in effluent. It is known to block the iodine uptake by thyroid gland. Is a detoxification product of hydrogen cyanide [6,146]. It has been used in the body fluid to monitor hydrogen cyanide from tobacco smoke, fire atmospheres and some vegetables containing cyanogenic glucosides [147]. In addition to the use of modified metallic electrodes, a number of researchers [146,148,149] are using ion selective electrode to determine thiocyanate. Unsubstituted iron-phthalocyanine, FePc [150], has also been used as a modifier to analyze thiocyanate in human urine and saliva samples.

REFERENCES

1. S. Iijima, *Nature* 354 (1991) 56.
2. P. G. Wiles, J. Abrahamson, *Carbon* 6 (1978) 341.
3. P. J. Britto, K. S. V. Santhanam, P. M. Ajayan, *Bioelectronics and Bioenergertics* 41 (1996) 121.
4. J. Wang, *Electroanalysis* 17 (2005) 7.
5. B. S. Flaven, J. Yu, A. V. Ellis and J. G. Shapter, *Electrochim. Acta* 54 (2009) 3191.
6. K. I. Ozoemena and T. Nyonkong, *Encyclopedia of Sensors* (ed.) C. A. Grimes, E. C. Dickey, and M. V. Pishko 3 (2006) 157.
7. M. Sekota and T. Nyonkong, *Polyhedron* 16 (1997) 3279.
8. S. Vilakazi and T. Nyonkong, *Polyhedron* 19 (2000) 229.
9. J. Limson and T. Nyonkong, *Electroanalysis* 9 (1997) 255.
10. M. Thamae and T. Nyonkong, *J. Elecrtoanal. Chem*. 470 (1999) 126.
11. S. Grieve, G. Pavez, J. H. Zagal and F. Bedioui, *J. Electroanal. Chem*. 497 (2001) 75.
12. B. O. Agboola and K. I. Ozoemena, *Phys. Chem. Chem. Phys* 10 (2008) 2399.
13. J. M. Lehn, *Supramolecular chemistry,* VCH Weinhein (1995).

14. J. N. Richardson, S. R. Peck, L. S. Curtin, L. M. Tender, R. H. Terrill, M. T. Carter, R. W. Murray, G. K. Rowe and S. E. Creager, *J. Phys. Chem.* 99 (1995) 766.

15. K. Weber, L. Hockett and S. E. Creager, *J. Phys. Chem. B* 101 (1997) 8286.

16. S. E. Creager and G. K. Rowe, *Anal. Chim. Acta* 246 (1991) 233.

17. S. E. Creager and G. K. Rowe, *Langmuir* 9 (1993) 2330

18. J. J. Gooding, A. Chou, J. Liu, D. Losic, J. G. Shapter, D. B. Hibbert, *Electrochem. Commun.* 9 (2007) 1677.

19. P.M. S. Monk, *Fundamentals of Electroanalytical Chemistry*, John Wiley and Sons Ltd, Chichester, New York (2001)

20. P. T. Kissinger, C. R. Preddy, R. E. Shoup and W. R. Heineman in *Laboratory Techniques in Electroanalytical Chemistry* 2nd ed., P. T. Kissinger and W. R. Heineman, Eds.; Marcel Dekker Inc., New York 1996.

21. J. Wang, Analytical *Electrochemistry*, VCH Publishers Inc. New York (1994).

22. D. B. Hibbert, *Introduction to Electrochemistry*, Macmillan, London (1993).

23. A. E. Kaifer and M. Gómez-Kaifer, *Supramolecular Electrochemistry*, Wiley-VCH, New York (1999).

24. A. J. Bard, L. R. Faulkner, *Electrochemical methods: Fundamental and applications*, 2nd ed., John Wiley and Sons, Hoboken, NJ, (2001).

25. C. Kittel, *Thermal physics*, 3rd edn, Wiley, New York (1969) 215.

26. G. Inzelt, Kinetics of electrochemical reactions. In: Scholz F (ed) *Electroanalytical methods* Springer, Berlin (2002) 38.

27. P. A. Christenson and A. Hamnet, *Techniques and Mechanisms in Electrochemistry*, 1st ed, Blackie Academic and Professional, London (1994).

28. J. E. B. Randles, *Trans. Faraday Soc*. 44 (1948) 327.

29. R. S. Nicholson and I. Shain, *Anal. Chem*. 36 (1964) 1351.

30. A. Sevcik, Coll. Czech. *Chem. Comm*. 13 (1958) 349.

31. J. Wang, *Analytical Electrochemistry*, 3rd ed, Wiley-VCH John Wiley & Sons Publishers Inc., Hoboken, New Jersey (2006).

32. E. R. Brown and R. F. Large, *in Physical Methods of Chemistry, Vol.1-Part IIA:Electrochemical Methods*, eds. A. Weissberger and B. Rossiter, Willey-Interscience, New York (1971).

33. F. M. Hawkridge in P. T. Kissinger and W. R. Heineman (Eds), *Laboratory techniques in electroanalytical chemistry*, 2nd ed., Marcel Dekker Inc., New York (1996).

34. J. Wang, *Analytical Electrochemistry*, VCH Publishers Inc., New York (1994).

35. J. Wang, D. B. Luo, P. A. M. Farias and J.S. Mahmoud, *Anal. Chem.* 57 (1985) 101.

36. J. G. Osteryoung, *Acc. Chem. Res*. 26 (1993) 77.

37. J. G. Osteryoung and R. A. Osteryoung, *Anal. Chem*. 57 (1985) 101A.

38. J. A. Turner, J. H. Christie, M. Vukovic, R. A. Osteryoung, *Anal. Chem*. 49 (1977) 1904.

39. G. C. Barker, A. W. Gardner, *J. Electroanal. Chem*. 100 (1979) 641.

40. S. Komorsky-Lovric, M. Lovric, M. Branica, *J. Electroanal.Chem*. 241 (1988) 329.

41. H. B. Oldham and J. C. Mayland, *Fundamentals of electrochemical science*, Academic press, San Diego (1994).

42. P. H. Rieger, *Electrochemistry*, Prentice Hall, Oxford (1987) 151.

43. A. J. Bard (ed) *Electroanalytical Chemistry*, Marcel Dekker, New York 13 (1994) 191.

44. A. J. Bard (ed) Electroanalytical Chemistry, Marcel Dekker, New York 18 (1994) 89.

45. R. G.Compton and C. E. Banks, *Understanding Voltammetry*, World Scientific Publishing Co. Pte. Ltd (2007).

46. J. Ni, H. Ju, H. Chen and D. Leech, *Anal. Chim. Acta* 378 (1999) 151.

47. A. J. Bard, G. Inzelt and F. Scholz, *Electrochemical dictionary*, Springer (2008).

48. R. D. Rocklin and R. W. Murray, *J. Phys. Chem.* 85 (1981) 2104.

49. F. Zhi, X. Lu., Y. Jiandong, X. Wang, H. Shang, S. Zhang, X. Zhonghua, J. Phys. Chem. C 113 (2009) 13166.

50. C. Chuangye, S. Yonghai; L. Wang, Electro. Chim. Acta 54 (2009) 1607.

51. R. G. Gonzalez-Huerta, A. R. Pierna, O. Solorza-Feria, J. New Mat. Electrochem. Syst. 11 (2008) 63.

52. I. Kazufumi, N. Katsuhiko, T. Isao, Chem. Lett. 38 (2009) 686.

53. R. N. Goyal, V. K. Gupta, S. Chatterjee, Biosensors & Bioelectronics 24 (2009) 3562.

54. M. H. Smit, C. A. Rechnitz, *Anal. Chem.* 64 (1992) 245.

55. X. Cai, K. Kalcher, C. Neuhold, W. Diewald, R. J. Magee, *Analyst* 118 (1993) 53.

56. S. M. Golabi, J. B. Raoof, *J. Electroanal. Chem*. 46 (1996) 75.

57. S. A. Wring, *Analyst* 117 (1992) 1215.

58. R. A. Durst, A. J. Baumner, R. W. Murray, R. P. Buck and C. P. Andrieux, *Pure Appl. Chem.* 69 (1997) 1317.

59. K. A. Peterlinz and R. Goergiadis, *Langmuir* 12 (1996) 4731.

60. B. Fang, X. H. Deng, X. W. Ken, H. S. Tao, W. Z. Zhang and M. G. Li, *Anal. Lett.* 39 (2006) 697.

61. J. Yu, J.G. Shapter, M. R. Johnston, J. S. Quinton, and J. J. Gooding, *Electrochim. Acta.* 52 (2007) 6206.

62. M. D. Porter, T. B. Bright, D. L. Allara, and C. E. D. Chidseyi, *J. Am. Chem. Soc*. 109 (1987) 1559.

63. R. G. Nuzzo, B.R. Zegarski and L. H. Dubois, *J. Am. Chem. Soc*. 109 (1987) 733.

64. L. H. Dubois and R. G. Nuzzo, *Ann. Rev. Phys. Chem*. 43 (1992) 437.

65. S. Griveau, J. Pavez, J. H. Zagal and F. Bedioui, *J. Electroanal. Chem.* 497 (2001) 75.

66. K. I. Ozoemena and T. Nyonkong, *Talanta* 67 (2005) 162.

67. G. M. Whiteside and B. Grzybowski, *Science* 295 (2002) 2418.

68. G. R. Desiraju*, Crystal Engineering: The Design of Organic Solids*, Elsevier, New York (1989).

69. L. Isaacs, D. N. Chin, N. Bowden, Y. Xia, G. M. Whitesides, *Supramolecular Technology,* D. N. Reinhoudt, Ed., Wiley, New York (1999) 1-46.

70. R. K. Shervedani, M. Bagherzadeh and S. A. Mozaffari, Sens. Actuators B 115 (2006) 614.

71. H. Wang, S. Chen, L. Li and S. Jiang, Langmuir 21 (2005) 2633.

72. R. K. Shervedani and S. A. Mozaffari, *surf. Coat. Technol.* 198 (2005) 123.

73. Y. I. Skurlatov, L. S. Ernestova, E. V. Vichutinskaya, D. P. Samsonov, I. V. Semenov, I. Y. Rod'ko, V. O. Shvidky, R. I. Pervunina and T. J. Kemp, *J.Photochem.Photobiol.* 107 (1997) 207.

74. W. A. Nevin, W. Liu, S. Greenberg, M. R. Hempstead, S. M. Maruccio, M. M. Melnik, C. C. Leznoff and A. B. P. Lever, *Inorg. Chem*. 26 (1987) 291.

75. H. O. Finklea in *Electroanalytical Chemistry*, A. J. Bard and I. Rubinstein, Eds., Marcel Dekker: New York 19 (1996) 109.

76. H. O. Finklea in R. A. Meyers, Eds., *Encyclopaedia of Analytical Chemistry: Applications, Theory and Instrumentations*, Vol. 11, Wiley, Chichester (2000) 10090.

77. D. Losic, J. G. Shapter and J. J. Gooding, *Langmuir* 17 (2001) 3307.

78. K. C. Nirmalya, M. Aslam, J. Sharma and K. Vijayamohanan, *Proc. Indian Acad. Sci (Chem. Sci.)* 113 (2001) 659.

79. M. Mrksich, G. M. Whitesides, *Annu. Rev. Biomol. Struct.* 25 (1996) 55.

80. J. J Gooding, V. Praig and E. A. H Hall, *Anal. Chim. Acta* 70 (1998) 2396.

81. Y. Okahata, Y. Matsunobu, K. Ijiro, M. Mukae, A. Murakami and K. Makino, *J. Am. Chem. Soc.* 114 (1992) 8299.

82. W. Wang, J. J. Gooding and D. B. Hibbert, *J. Electroanal. Chem.*516 (2001)10.

83. H. O. Finklea and D. D. Hansheu, *J. Am. Chem. Soc.* 114 (1992) 3173.

84. A. M. Becka and C. J. Miller, *J. Phy. Chem.* 96 (1992) 2657.

85. Y. H Tse, P. Janda and A. B. P. Lever, *Anal. Chem.* 66 (1994) 384.

86. T. F. Kang, Z. Y. Xie, H. Tang, G. L. Shen and R. Q. Yu, *Talanta* 45 (1997) 291.

87. M. Thamae and T. Nyonkong, *J. Electroanal. Chem.* 470 (1999) 126.

88. T. Mafatle and T. Nyonkong, *Anal. Chim. Acta.* 354 (1997) 307.

89. C. A. Caro, F. Bedioui and J. A. Zagal, *Electro. Chim. Acta* 47 (2002) 1489.

90. A. J. Bard, J. Chem. Ed. 60 (1983) 302.

91. I. Zilbermann, J. Hayon, T. Katchalski, R. Ydgar, J. Rishpon, A. I. Shames, E. Korin and A. Bettelheim, *Inorg. Chim. Acta.* 305 (2000) 53.

92. M. J. Cook, J. Mater. *Chem.* 6 (1996) 677

93. M. J. Cook, *Pure Appl. Chem*. 71 (1999) 2145.

94. A. Ulmann, *An introduction to ultrathin organic films from Langmuir-blodgett to self-assembly*, Academic Press, San Diego (1991).

95. H. Li, T. F. Guarr, *J. Chem.Soc. Chem.Commun.* (1989) 832.

96. J. M. Robertson, *J. Chem. Soc.* (1936) 1195.

97. P. Gregory, *J. Porphyrins Phthalocyanines* 3 (1999) 468.

98. N. B. McKeown, *Chem. Ind.* (1999) 92.

99. T. Nyokong, Z. Gasyna and M.J. Stillman, *Inorg. Chem.* 26 (1987) 548.

100. J. Simon and P. Bassoul, *Phthalocyanine: Properties and Applications,*Leznoff, C.C., Lever, A.B.P., Eds. V.H.S. Publishers: New York (1989).

101. P. Gregory in *High Technology Applications of Organic Colorants*, Plenum Press, New York (1991).

102. J. E. Kuder, *J. Imaging Sci*., 32 (1988) 51.

103. R. Ao, L. Kummert and D. Haarer, *Adv. Mater*. 5 (1995) 495.

104. H. S. Nalwa and J. A. Shirk in *Phthalocyanine: Properties and Applications,*(A. P. B. Lever and C. C. Leznoff, Eds), VCH Publishers, New York 4 (1996) 79.

105. E. Ben-Hur and I. Rosenthal, *Int. J. Radiat. Biol*. 47 (1985) 145.

106. E. Ben-Hur and I. Rosenthal, *J. Photochem. Photobiol*. 42 (1985) 129.

107. I. Rosenthal and E. Ben-Hur, *in Phthalocyanine: Properties and Applications,*eds. A.P.B. Lever and C.C. Leznoff, VCH Publishers, New York, 1 (1989).

108. D. Phillips, *Pure Appl. Chem*. 67 (1995) 117.

109. I. J. MacDonald and T. Dougherty, *J. Porphyrins Phthalocyanines* 5 (2001) 105.

110. A. B. P. Lever, M. R. Hempstead, C. C. Leznoff, W. Lui, M. Melnik, W. A Nevin and P. Seymour, *Pure Appl. Chem*. 58 (1986) 1467.

111. K. Morishige, S. Tomoyasu and G. Iwano, *Langmuir* 13 (1997) 5184.

112. A. W. Snow and W.R. Barger in *Phthalocyanines: Properties and Applications* eds. A.P.B. Lever and C.C. Leznoff, VCH Publishers, New York 1 (1989).

113. S. Vilakazi and T. Nyokong, *Polyhedron* 19 (2000) 229.

114. T. Nyonkong and S. Vilakazi, *Talanta* 61 (2003) 27.

115. J. H. Zagal, *Coord. Chem. Rev.* 119 (1992) 89.

116. S. Top, A. Vessières, G. Leclercq, J. Quivy, J. Tang, J. Vaissermann, M. Huché and G. Jaouen, *Chem. Eur.J.* 9 (2003) 5223.

117. H. B. Kraatz, J. Lusztyk and G. D. Enright, *Inorg. Chem.* 36 (1997) 2400.

118. P. Saweczko, H. -B. Kraatz, *Coord. Chem. Rev.* 190 (1999) 185.

119. P. Allan and L. Jason, Chem Rev. 7 (1997) 6.

120. Z. K. Tang, Z. Lingyun, N. Wang, X. X. Zhang, G. H. Wen, G. D. Li, J. N. Wang, C. T. Chan and P. Sheng, *Science* 292 (2001) 2462

121. R. G. Ding, G. Q. Lu, Z. F. Yan, and M. Wilson, *J. Nanosci. Nanotechnol.* 1 (2001) 7.

122. P. Ball, *Nature* 414 (2001) 142.

123. P. Kim and C. M. Lieber, *Science* 286 (1999) 2148.

124. O. Stephan, P. M. Ajayan, C. Colliex, Ph. Redlich, J. M. Lambert, P. Bernier, P. Lefin, *Science* 266 (1994) 683.

125. R. Sen, B. C. Satishkumar, A. Govindaraj, K. R. Harikumar, G. Raina, J. -P. Zhang, A. K. Cheetham, C. N. R. Rao, *Chem. Phys.Lett.* 287 (1998) 671.

126. M. Yudasaka, R. Kikuchi, Y. Ohki, S. Yoshimura, *Carbon 35* (1997) 195.

127. S. H. Lai, Y. L. Chen, L. H. Chan, Y. M. Pan, X. W. Liu, H. C. Shih, *Thin Solid Films* 444 (2003) 38.

128. S. G. Louie, *Top. Appl. Phys*. 80 (2001) 113.

129. R. Camacho, A. Morgan, M. Flores, T. McLeod, V. Kumsomboone, B. Mordecai, R. Bhattacharjea, W. Tong, B. Wagner, J. Flicker, S. Turano, W. Ready, *J. Min. Metals and Mater. Soc.* 59 (2007) 39.

130. B. A. Boukamp, *Solid States Ionics* 18 and 19 (1986) 136.

131. S. Khene, D. A. Geraldo, C. A. Togo, J. Limson and T. yonkong, *Electro. Chim. Acta.* 54 (2008) 183.

132. C. M. Brett, A. M. O. Brett, *Electrochemistry: Principle, methods and Applications*, Oxford University Press, New York, USA (1993).

133. S. Krause, Impedance methods, in A. J. Bard, M. Stratmann, P. R. Unwin (Eds), *Encyclopedia on Electrochemistry*, vol 3, Wiley-VCH, Weinheim, Germany (2003).

134. Y. Yang, S. B. Khoo, *Sens. Actuators B* 97 (2004) 221.

135. X. Ren, P. J. Puckup, *J. Electroanal. Chem.* 420 (1997) 251.

136. A Chidembo, B. A. Agboola, V. Gupta, G. G. Wildgoose, R. G. Compton and K. I. Ozoemena, Chem. Commun. (2009) in press.

137. D. D. MacDonald, *Electrochim. Acta*, 51 (2006) 1376.

138. G. Binning, C. F. Quate and C. Gerber, Phys. Rev. Lett. 56 (1986) 930.

139. H. Hansma, A. Weisenhorm, A. Edmundson, H. Gaub and P. Hansma, *Clin. Chem*. 37 (1991) 1497.

140. C. E. Gardner, J. V. Macpherson, *Anal. Chem.* 74 (2002) 576A.

141. C. R. Blanchard, *The chemical educator* 1 (1996) 1.

142. Y. A. Novikov, Y. V. Ozerin, A. V. Rakov and P. A. Todua, Measurement Sci. Technol. 18 (2007) 367.

143. S. Guenu, A. E. Heng, F. Charbonne, M. J. Galmier, F. Charles, P. Deteix, B. Souweine and C. Lartigue, Rapid Comm. Mass Spectrom. 21 (2007) 229.

144. D. Briggs and M. P. Seah, Practical Surface Analysis by Auger and X-Ray Photoelectron Spectroscopy, Eds. New York: Wiley 1983

145. J. Javier, S. Heriban and N. Fabiola, *Regeneration of Cyanide by oxidation of thiocyanate* (1996) US Patent 5482694.

146. K. A. Singh, U. P. Singh, S. Mehtab and V. Aggarwal, *Sens. Actuators* B 125 (2007) 453.

147. J. A. Cox and T. Gray, *Anal. Chem.* 60 (1988) 1710.

148. A. Abbaspour, M. A. Kamyabi and R. K. Esmaeilbeig, *Talanta* 57 (2002) 859.

149. M. K. Amini, S. Shahrokhian, and S. Tangestaninejad, *Anal. Chim. Acta.* 402, (1999) 137.

150. K. O. Ozoemena and T. Nyonkong, *J. Electroanal. Chem.* 579 (2005) 283.

CHAPTER 2

EXPERIMENTAL

2.1. Introduction

This chapter describes the reagents and their grades, as well as the equipments used to carry out the experiments reported in this thesis. The method used to functionalize carbon nanotubes is reported in details. Also, described are the characterization techniques employed in this project, namely SEM, XPS, AFM and EDX.

2.2. Reagents and material

Table 2.1 lists the reagents used and their purity or composition in weight %. The reagents were of analytical grade and were used as received from the suppliers without further purification.

Gold electrode of radius 0.8 mm from Bioanalytical systems (BAS), the rotating disk electrode consists of a 5 mm gold disk of radius 2.5 mm embedded in a cylindrical insulating material (e.g Teflon) were obtained from Eco Chemie. The electrodes were cleaned before forming the SAM following the same procedure described below for the normal electrode of radius 0.8 mm. ITO-gold nanoparticles (used as received).

Saliva samples of smokers and non-smokers were donated by colleagues at the University of Pretoria. 1 ml of saliva sample was diluted to 1:10 with pH 4.8 phosphate buffer. The resulting mixture was used directly for determination of thiocyanate ion concentration.

Table 2.1: List of reagents, their purity and suppliers

Reagents	Purity or composition (wt%)	Supplier
Alumina		Sigma
Cobalt tetraaminophthalocyanine(II)[a]	—	—
Cysteamine hydrochloride	98.0	Fluka
Dicyclohexylcarbodiimide	99.0	Aldrich
N,N-dimethylformamide	99.0	SAARCHEM
Ethanol	99.5	SAARCHEM
Ferrocenecarboxylic acid	97.0	Fluka
1,1-Ferrocene-dicarboxylic acid	96.0	Aldrich
Hydrogen peroxide	30.0	SAARCHEM
Iron tetraaminophthalocyanine(II)[a]	—	—
Nitric acid	65.0	A C E
Ortho-Phosphoric acid	85.0	SAARCHEM
Octa(hydroxyethylthio)phthalocyaninatoiron(II)[a]		—
Potassium chloride	99.0	RADCHEM
Potassium ferrocyanide	98.0	B.O. Jones LTD
Potassium ferricyanide	98.0	Bio-zone chemicals
Potassium thiocyanate	—[b]	A C E
Single-walled carbon nanotubes	70.0	Aldrich
Sodiumdihydrogenphosphate-1-hydrate	99.0	MERCK
Sodium hydroxide	98.0	Bio-zone chemicals
di-Sodiumhydrogenphosphate	98.0	MERCK
Sulphuric acid	98.0	BDH

[a]used as received
[b]purity not specified

2.2.1. Functionalization of carbon nanotubes

Purification method described by Smalley *et al*. [1], was used to functionalize the carbon nanotubes. Functionalisation strategy involves multistep processes to yield SWCNTs with carboxylic acid functional groups ready for further chemistry (SWCNT-COOH). The multistep process begins with 24 hr reflux in 2.6 $mol.l^{-1}$ of 65% nitric acid. After cooling, the mixture was centrifuged at 3000 rpm leaving black sediment at the bottom of the centrifuge bottles and a clear brownish-yellow supernatant which is decanted off. The sediment still contained substantial trapped acid which is removed by repeatedly washing the sediment with deionized water. This step was followed by a 24 hr sonication at 40°C in a mixture of 3:1 H_2SO_4 and HNO_3. Again the mixture was washed by means of centrifuge and dried at 30^{o}C overnight. Finally the SWCNT-COOHs were centrifuged in a mixture of 4:1 ratio H_2SO_4 and H_2O_2, washed with deionised water and monitor pH every after wash using indicator sticks until the solution's pH approaches 7.0, filtered and dried at 30^{o}C overnight. All experiments were performed at 25±1 °C.

2.3. Instrumentation

Voltammetric and amperommetric measurements were carried out using Advanced Electrochemical System, Autolab potentiostat PGSTAT 100/30 (Eco Chemie, Utretch, The Netherlands) driven by the General Purpose Electrochemical Systems data processing software (GPES, software version 4.9) equiped with a three electrode set-up consisting of either bare gold electrode (r = 0.8 mm, BAS) or the same gold electrode modified with the investigated SAMs, as working electrode, Ag|AgCl wire as pseudo reference electrode and platinum wire as counter electrode. Square wave parameters were: step potential 5 mV; equilibration time 5 sec, amplitude 25 mV at a frequency of 15 Hz. Electrochemical impedance spectroscopy (EIS) measurements were performed with Autolab Frequency Response Analyser (FRA) software between 10 kHz and 10 mHz using a 5 mV rms sinusoidal modulation in phosphate buffer solutions of different pH values of 1 mM of $K_4Fe(CN)_6$ and 1 mM $K_3Fe(CN)_6$ (1:1) mixture containing 0.1 M KCl at the $E_{1/2}$ of the $[Fe(CN)_6]^{3-/4-}$ (0.1 V vs Ag|AgCl). Solutions were deoxygenated by a stream of high purity nitrogen for at least 5 min before running the experiment and the solution was protected from air by a blanket of nitrogen during the experiment. Using the $[Fe(CN)_6]^{3-/4-}$ reversible electrochemistry at scan rates ranging from 0.01 to 0.20 Vs^{-1} and employing the Randles

Sevčik theory [2,3], the electrochemical roughness factor of the gold electrode (i.e. ratio o fthe real (0.027cm^2) to geometric (0.020cm^2) used for this report was determined to be *ca.* 1.34. Before electrochemical examination of each of the modified electrode, the electrode was first pretreated by repetitive cycling (20 scans) in 0.5 M H_2SO_4 until a reproducible scan was obtained.

A BENCHTOP, 420A (LABOTEC) pH meter was used for pH measurements. Ultra pure water of resistivity 18.2 MΩ.cm was obtained from a Milli-Q Water System (Millipore Corporation, Bedford, MA, USA) and was used throughout for the preparation of solutions. Ultrasonic bath (INTEGRAL SYSTEMS) was used for sonication.

Surface images were acquired with atomic force microscopy (AFM) 5100 System (Agilent Technologies, USA) using AC mode AFM scanner interfaced with a PicoScan 5.0 controller. Silicon type PPP-NCH-20 (Nanosensors®) of thickness 4.0±1.0 µm, length 125±10 µm, width 30±7.5 µm, spring constants 10-130 N m^{-1}, resonant frequencies of 204–497 kHz and tip height of 10-15 µm were used. All images were taken in air at room temperature in anti-vibration chamber. Gold coated glass was cleaned by placing the glass in pinraha solution for 2 min, then rinsed with Millipore water, dried with air nitrogen and immediately immersed in desired solution to form SAM. After Sam formation the electrode was then rinsed with Millipore

water followed by ethanol and dried in nitrogen and placed in a sample chamber for scanning. Field emission electron microscopy (FESEM) images were obtained from JOL JSM 5800 LV (Japan). Morphological analyses of the different SAMs were carried out and viewed at an accelerating voltage of 5 kV and using the lowest beam current in order to avoid sample damage. Small amounts of sample material were transferred into a test tube. About 5ml of ethanol were added to the test tube which was then placed in an ultrasonic bath (bramsonic bath 5200) for about 30 sec to separate the sample particle and produce a suspension of fine particle. Small amounts of the suspension were extracted with 2 mL disposable polyethylene Pasteur pipette and transferred onto a conducting adhesive carbon tab (12 mm diameter) which were attached to an aluminium stub. The alcohol was allowed to evaporate in an oven at 30^{o}C.

X-ray photoelectron spectroscopy (XPS) measurements were carried out using a physical electronics model 5400 spectrometer system at a vacuum of abour 10^{-8} Torr, with monochromatic Mg Kα radiation at 1253.6 eV. Take-off angle of 20, 45 and 80^{o} were used for the studies. All spectra were averages of 20 scans of 60 sec duration. The binding energies for all thin film samples were referenced to the 1s carbon peak at 284.5 eV. The experiments were performed with gold-coated glass slides as substrates for the SAMs.

2.4. Electrode modification procedure

2.4.1. Electrode pre-treatment

The gold electrodes used were first cleaned following the conventional procedure [4,5]. For each experiment the electrode was polished in an aqueous slurry of alumina (<10 μm) on a SiC-emery paper (type 2400 grit), and then to a mirror finish on a Buehler felt pad. The electrode was then subjected to ultrasonic vibration in absolute ethanol to remove residual alumina particles that might be trapped at the surface. Finally the electrode was etched for about 2 min in a hot 'Piranha' solution (1:3 (v/v) 30% H_2O_2 and concentrated H_2SO_4) for about 1 min, and then rinsed with copious amounts of ultrapure Millipore water followed by ethanol. This stage was necessary to remove organic contaminants and was followed by thorough rinsing with distilled water. The cleanliness of the bare electrode surface was finally established by placing it in 0.5 M H_2SO_4 and scanning the potential between −0.5 and 1.5 V (vs Ag|AgCl wire) at a scan rate of 0.05 Vs^{-1} until a reproducible scan was obtained.

***CAUTION**: Piranha solution must be handled with care as it reacts violently with organic materials and can explode when stored in closed containers*.

2.4.2. Self-assembling technique

2.4.2.1 SWCNT-phthalocyanine based electrode

The formation of reproducible self-assembled monolayers (SAM) requires a reproducible surface. Following the pre-treatment, the electrode was placed in nitrogen-saturated 10 mM solutions of cysteamine hydrochloride to allow the Au-Cys electrode to form for a desired period of time. Then the electrode was thoroughly rinsed with absolute ethanol solution before reacting with SWCNT. A 3 mg of acid treated SWCNT was first dispersed in 1 ml pure dry DMF with 0.5 mg DCC (2.4μmol) to convert the –COOH groups at the ends of the SWCNT into active carbodiimide esters. The surface condensation of the Au-Cys electrode was achieved by placing the electrode in the black solution of SWCNT/DCC/DMF for 24 hr. The condensation of the –COOH functional groups of the SWCNT with the $-NH_2$ groups of the Cys SAM resulted in the formation of the amide bonds [6-8].

The FeOHETPc was attached to the free DCC-activated ends of the SWCNT by placing the Au-Cys-SWCNT electrode in a DMF solution containing ~ $1.0x10^{-3}$ M FeOHETPc for 25 hr. The surface of the Au-Cys-SWCNT electrode is expected to contain some active carbodiimide esters that would be attacked by the hydroxyl functional groups of the FeOHETPc to generate the SWCNT-FeOHETPc via ester bonds,

releasing dicyclohexylurea (DCU) in the deposition solution [9]. Facile esterification of the –OH functionality through carbodiimide couplings is well documented [10-12] and more recently, in selective esterification of the -OH of the mercarptoethanol functionality with the free -COOH of the SWCNT SAM. The experiments were carried out using nitrogen purged solutions of either H_2SO_4 for pretreatment or analyte in phosphate buffer (pH 4.8) using gold electrode modified with the complexes as the working electrodes while Ag|AgCl and platinum electrodes were employed as reference and counter electrodes, respectively.

2.4.2.2 SWCNT-ferrocene based electrodes

Self-assembled monolayers of alkanethiol capped with carboxylated ferrocene and single-walled carbon nanotubes were prepared on gold surfaces. Following the formation of Au-Cys electrode for 18 hr, the electrode was rinsed with ultrapure water and dried with nitrogen. The formation of Au-Cys-FDCA and Au-Cys-FMCA followed after placing the Au-Cys electrode in a 1ml DMF solution containing 3mg FDCA or FMCA for 48 hr, respectively.

The Au-Cys-SWCNT/FDCA electrode was obtained simply by placing Au-Cys in DMF solution containing equimolar mixture of SWCNT and FDCA and 0.5 mg DCC for 48 hr. This same method was

used to prepare Au-Cys-SWCNT/FMCA. Upon removal from the deposition solution, prior to electrochemical experiments, the electrode was thoroughly rinsed with millipore water and dried in a nitrogen atmosphere.

Prior to electrochemical experiments, the modified electrodes were conditioned by placing in 0.5 M H_2SO_4 and repetitively scanned between −0.5 and 0.6 V (vs Ag|AgCl) potential window at a scan rate of 25 mVs^{-1} until a constant scan was obtained.

2.4.2.3 Nano-gold indium tin oxide electrode

The gold nanoparticles were deposited on indium tin oxide surface by the method described by Kambayashi *et al*. [13]. The electrodes were kindly donated by Prof. Munetaka Oyama of the chemistry department of Kyoto University, Japan. The SEM images of these electrodes, (see Figure 2.1), shows the attached gold nanoparticles in which the SAM was anchored. Formation of the SAM follows the described procedure (see chapter 3) where ITO-nanoAu was deposited to a nitrogen-saturated absolute ethanol solution of cysteamine for 4 hr. After rinsing, the electrode was immediately placed into a mixture of SWCNT/FDCA for 2 hr to form nanoAu-Cys-SWCNT/FDCA electrode and the electrode was ready for use.

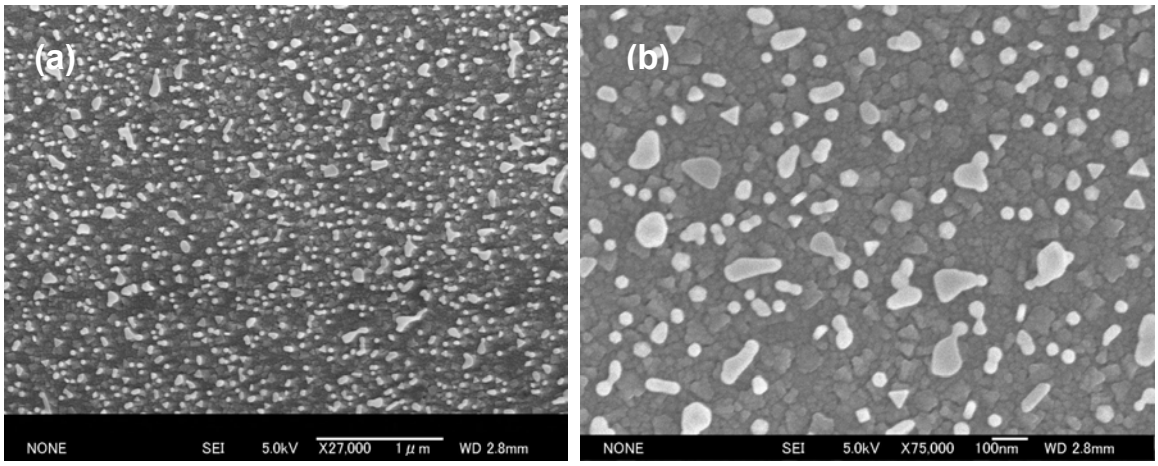

Figure 2.1: FESEM images of the nanogold modified ITO electrode (a) 1 μm magnification and (b) 100 nm magnification. (Duplicated with permission from Oyama and co-workers [13]).

REFERENCES

1. R. E. Smalley, A. G. Rinzler, J. Liu, H. Dai, P. Nikolaev, C. B. Huffman, F. J. Rodriguez-Macias, P.J. Boul, A. H. Lu, D. Heymann, D. T. Colbert, R. S. Lee, J. E. Fischer, A. M. Rao, P. C. klund, Appl. Phys. A 67 (1998) 29.
2. A. J. Bard, L. R. Faulkner, Electrochemical Methods: Fundamentals and Applications, 2nd ed., John Wiley & Sons, Hoboken, NJ. 2001
3. H. O. Finklea in R. A. Meyers, Eds., *Encyclopaedia of Analytical Chemistry:Applications, Theory and Instrumentations*, Vol. 11, Wiley, Chichester (2000) 10090.
4. P. Diao, Z. Liu, J. Phys. Chem. B. 109 (2005) 20905.
5. Z. F. Liu, Z. Y. Shen, T. Zhu, S. F. Huo, L. Z. Ying, Z. J. Shi and Z. N. Gu, Langmuir 16 (2000) 3569.
6. J. J. Gooding, R. Wibowo, J. Liu, W. Yang, D. Losic, S. Orbons, F. J. Meams, J.G. Shapter, D. B. Hibbert, *J. Am. Chem. Soc.* 125 (2003) 9006.
7. F. Patolsky, Y. Weizmann, I. Willner, *Angew. Chem. Int*. Ed. 43 (2004) 2113.
8. L. Sheeney-Haj-Ichia, B. Basnar, I. Willner, *Angew. Chem. Int*. d. 44 (2005) 78.

9. P. Y. Bruice, *Organic Chemistry*, fiftth ed., Person Prentice Hall, New Jersey, chapter 22 (2007) 1041.

10. B. Neiss, W. Steglich, *Org. Synth*. 63 (1985) 183.

11. R. Shelkov, M. Nahmany, A. Melman, *Org. Biomol. Chem*. 2 (2004) 397.

12. J. Yu, J. G. Shapter, J. S. Quinton, M. R. Johnston, D. A. Beattie, *Phys.Chem.Chem.Phys.* 9 (2007) 510.

13. J. Zhang, M. Kambayashi, M. Oyama, *Electrochem. Commun.* 2004, 6, 683.